Femtosecond photon echoes in molecular aggregates

T. Meier, V. Chernyak, and S. Mukamel
Department of Chemistry and Rochester Theory Center for Optical Science and Engineering, University of Rochester, Rochester, New York 14627

(Received 25 March 1997; accepted 7 May 1997)

Two-pulse four-wave-mixing signals from molecular aggregates, including effects of two-exciton states, static disorder, and exciton-phonon interaction represented by arbitrary spectral densities are calculated. Three types of contributions to the signal are identified. The first, reflecting exciton self-correlation, is similar to the photon echo from disordered two-level systems and dominates the signal for long time-delays. The second is related to correlations of one-exciton states, whereas the third reflects correlations between one- and two-exciton states. The information gained by completely resolving the signal field (both amplitude and phase) is analyzed using Wigner spectrograms. © *1997 American Institute of Physics.* [S0021-9606(97)02031-X]

I. INTRODUCTION

Molecular aggregates have recently become an object of extensive studies using a variety of ultrafast nonlinear spectroscopic techniques.[1–7] Despite a relatively simple structure of electronic excitations represented by Frenkel excitons (compared to inorganic semiconductor materials and conjugated polyenes), optical signals from molecular aggregates show signatures of complex physical phenomena: exciton-exciton scattering due to their repulsive (Pauli exclusion) and attractive (e.g., dipole-dipole) interactions, static disorder resulting in elastic scattering and exciton localization, whereas strong exciton-phonon coupling may induce inelastic exciton scattering and exciton-self trapping (also known as exciton dynamical localization). Coherent and incoherent exciton dynamics in J-aggregates[4–7] and in light harvesting complexes[2,3] has been probed by various time-domain optical measurements such as fluorescence depolarization,[8,9] hole burning,[10–13] pump-probe,[14–16] and photon echoes.[17,18] Interpretation of current experiments constitutes a complicated task since a theory which incorporates exciton-exciton interaction, strong exciton-phonon coupling, and static disorder is yet to be developed. Existing theories of nonlinear optical response in molecular aggregates are based on the Frenkel exciton Hamiltonian which describes an aggregate made out of two-level molecules and conserves the number of excitons. They can be classified according to the level of reduction with respect to nuclear (phonon) variables. At the lowest level one keeps electronic (excitonic) degrees of freedom only. Neglecting exciton-phonon coupling, exact expressions for the third-order nonlinear optical response have been derived[19] using equations of motion for one- and two-exciton variables. These equations are closed using the pure state factorization[1] of higher order variables. These expressions have been later recast in terms of the exciton-exciton scattering matrix.[20] For one-dimensional aggregates with nearest-neighbor intermolecular coupling, the third order nonlinear response functions have been alternatively calculated[21] using the sum-over states approach and the Wigner-Jordan representation for two-exciton states.[1,22] Both formulations have been successfully employed in calculations of optical signals from molecular aggregates and nanostructures, incorporating effects of static disorder by Monte-Carlo simulations.[21,23–26]

Exciton-phonon interactions have been included in the model[19] using equations of motion for exciton and phonon variables, with truncation of higher order members of the exciton hierarchy.[27] These equations can describe phonon-induced incoherent exciton motion which shows up in degenerate four-wave mixing and transient-grating techniques; however they do not include two-exciton states, and therefore apply only far from two-exciton resonances. A more profound maximum-entropy factorization,[28] has been proposed, which interpolates between the coherent and the incoherent limits. However it does not fully describe the combined effects of two-exciton resonances and exciton transport. A theory which describes these combined effects on third-order optical susceptibilities[25] was developed recently[29] using equations of motion for exciton variables, where exciton-phonon coupling was taken into account through relaxation operators, evaluated using projection operator techniques.[30,31] Closed Green function expressions (GFE) for the third-order response were obtained by using an approximate factorized form of relaxation operators, as opposed to previous schemes of Refs. 27,28 where factorization is imposed directly on the dynamical variables in the equations of motion. The same results were obtained earlier[25,32] using diagrammatic techniques with partial infinite-order resummations of the most important terms in the expansions of optical susceptibilities in the exciton-phonon coupling. The GFE and their generalizations[33] to aggregates made of three-level molecules have been recently applied to study the role of exciton-phonon coupling in the pump-probe signals from LH2 antenna complexes of purple bacteria.[34] Since exciton-phonon coupling is treated perturbatively through relaxation operators, the approach is limited to weak exciton-phonon coupling and is not sensitive to the detailed features of the nuclear spectral densities. This is a serious limitation for one-dimensional systems such as linear J-aggregates, and circular LH1 and LH2 antenna complexes, since even weak exciton-phonon coupling leads to a polaron formation[35] and weak static disorder results in Anderson

localization.[36] Effects of exciton localization and self-trapping (polaron formation) on relaxed fluorescence of LH2 antenna complexes have been studied in Ref. 37. However, that approach assumes that the aggregate is equilibrated in the excited state, and does not describe the time evolution of the signal.

On the other hand, the model of a single two-level chromophore coupled to a harmonic bath is exactly solvable and strong exciton-phonon coupling can be taken into account explicitly.[1,38] This model has been commonly used in the analysis of four-wave-mixing measurements.[39–41] A procedure which allows to treat the dynamics of aggregates strongly coupled to nuclear motions by identifying a few collective nuclear variables has been proposed.[42] This yields equations of motion for wavepackets representing the collective coordinates; solving these equations of motion remains however a demanding task.

In summary, there are three types of theories which describe the photophysics of molecular aggregates (i) theories which take into account the structure of electronic excitations explicitly using very simple models of exciton-phonon coupling, (ii) theories which treat exciton-phonon interactions explicitly, for a single electronically excited level, and (iii) theories which account for realistic structure of electronic excitations and collective nuclear dynamics. However, efficient numerical methods for solving the resulting equations of motion for wavepackets are yet to be developed.

The goal of this paper is to develop a theory of four-wave mixing in molecular aggregates which combines the advantages of (i) and (ii) and overcomes the numerical difficulties of (iii). This theory therefore corresponds to an intermediate level of description between (i), (ii), and the theory of (iii). The present theory takes into account realistic structure of electronic excitations together with detailed information about exciton-phonon coupling represented by spectral densities and static disorder. Our main assumption which simplifies the solution considerably is that effects of static disorder are stronger than exciton-phonon interactions. The theory is applied to the analysis of two-pulse four-wave-mixing in LH2 antenna complexes. This is an optical technique which allows the selective elimination of inhomogeneous broadening.[1] The nature of the two-pulse four-wave-mixing signal is well understood in the case of a two-level system where the echo originates from self correlation of the excited electronic state. The echo decay in the case of coupling to a harmonic bath can be calculated exactly.[1] Photon echoes in molecular aggregates do not have a simple physical interpretation since the electronic structure of the aggregate is more complicated and photon echoes reflect one-exciton state correlations and correlations between one- and two-exciton states. Photon echoes in disordered aggregates have been studied using analytical methods[25,43] in the weak localization limit, i.e. when one-exciton states are not localized and the localization length l_A is much larger than the disorder-induced mean free path. It has been shown that photon echoes in this situation originate from strong exciton correlations and can be conveniently described using multi-dimensional spectral densities.[25,44] However, the approach of Refs. 25, 43 treats exciton-phonon coupling on the simplest level by adding homogeneous dephasing, and therefore does not fully take into account effects of nuclear spectral densities. Nevertheless it gives insight into disorder-induced statistics of exciton levels.

The paper is organized is follows. In Sec. II we present the Frenkel exciton Hamiltonian coupled to a bath represented by arbitrary spectral densities, and give expressions for the third-order nonlinear optical response functions. Then in Sec. III we employ the exciton representation and derive expressions for the optical response, assuming that bath-induced nondiagonal coupling in the exciton representation may be neglected. Explicit formulas for various two-pulse four-wave-mixing signals including the time-integrated, time-resolved and frequency-resolved FWM signals, as well as the Wigner spectrogram, which is a mixed time-frequency representation, are given in Sec. IV. In Sec. V (see also Appendix C) we apply the results of Sec. IV to simple excitonic two-, three-, and four-level systems coupled to an overdamped Brownian-oscillator. The analysis of the different FWM signals provides insight into the dynamics induced by the combined effects of excitonic structure, exciton-phonon coupling, and static disorder. Numerical results for FWM signals from the B850 band of LH2, modeled as a ring consisting of 18 Bchl-a monomers,[45] with nearest-neighbor interactions, are presented in Sec. VI. Recent photon echo studies on photosynthetic antenna complexes LH1 and LH2[18] show the dependence of the time-integrated signals on the time delay. Experimental results have been interpreted using a two-level system coupled to a bath with complex spectral densities.[18] One important issue addressed in these calculations is whether the experimental results of Ref. 18 can be interpreted using a realistic structure of electronic excitations with a simple model of homogeneous exciton dephasing, and to what extent they provide a direct probe for the underlying spectral densities. We compare different models for exciton-phonon coupling and disorder and demonstrate their signatures in the optical signals. Our results are finally summarized in Sec. VII.

II. MODEL HAMILTONIAN AND NONLINEAR OPTICAL RESPONSE OF FRENKEL EXCITONS

We describe an aggregate made of two-level molecules coupled to a bath consisting of nuclear (intramolecular, intermolecular and solvent) degrees of freedom, using the Frenkel-exciton Hamiltonian[46]

$$H=\sum_n \Omega_n(\mathbf{q})B_n^\dagger B_n+\sum_{mn}^{m\neq n} J_{mn}(\mathbf{q})B_m^\dagger B_n+H_{ph}, \tag{1}$$

where B_n ($B_n^\dagger$) are exciton annihilation (creation) operators, with commutation relations

$$[B_m,B_n^\dagger]=\delta_{mn}(1-2B_m^\dagger B_m), \tag{2}$$

$H_{\rm ph}$ is the phonon Hamiltonian, and $\mathbf{q}$ represents the complete set of nuclear coordinates. Exciton-phonon coupling is incorporated through the $\mathbf{q}$-dependence of Ω_n and J_{mn}. The

polarization operator P representing coupling of the aggregate to the optical field $-E(t)\cdot P$ has a form

$$P=\sum_m d_m(B_m+B_m^\dagger), \tag{3}$$

where d_m is the transition dipole of the mth molecule. Adopting a harmonic model for the bath and expanding $\Omega_n(\mathbf{q})$ and $J_{mn}(\mathbf{q})$ to first order in $\mathbf{q}$, the Hamiltonian Eq. (1) can be partitioned in the form

$$H=H_e-\sum_{mn} q_{mn}^{(c)}B_m^\dagger B_n+H_{\rm ph}. \tag{4}$$

Here H_e is the exciton (system) Hamiltonian

$$H_e\equiv\sum_n \Omega_n B_n^\dagger B_n+\sum_{mn}^{m\neq n} J_{mn}B_m^\dagger B_n+H_{\rm ph}, \tag{5}$$

and $q_{mn}^{(c)}$ represent collective bath coordinates. All relevant information about the exciton-phonon interaction is contained in the following matrix of spectral densities:

$$C_{mn,kl}(\omega)\equiv\frac{i}{2}\int_{-\infty}^{\infty}dt\ \exp(i\omega t)\langle[q_{mn}^{(c)}(t),q_{kl}^{(c)}(0)]\rangle, \tag{6}$$

where the expectation value and the time evolution in the r.h.s. of Eq. (6) are taken with respect to the free phonon Hamiltonian $H_{\rm ph}$.

The time-domain optical response function $R(t_3,t_2,t_1)$ which relates the third-order nonlinear polarization $P^{(3)}(t)$ to the driving field $E(t)$ it defined by[1]

$$P^{(3)}(t)=i^3\int_0^\infty dt_3\int_0^\infty dt_2\int_0^\infty dt_1\ R(t_3,t_2,t_1)\times E(t-t_3)E(t-t_3-t_2)E(t-t_3-t_2-t_1). \tag{7}$$

The response function can be represented as of a sum of eight terms[1]

$$R(t_3,t_2,t_1)=\sum_{\alpha=1}^{4}[R_\alpha(t_3,t_2,t_1)-R_\alpha^*(t_3,t_2,t_1)], \tag{8}$$

Each of the contributions can be expressed in terms of the 4-point correlation function of the polarization operator

$$F(\tau_4,\tau_3,\tau_2,\tau_1)\equiv\langle P(\tau_4)P(\tau_3)P(\tau_2)P(\tau_1)\rangle. \tag{9}$$

We then have

$$\begin{aligned}
R_1(t_3,t_2,t_1)&\equiv\langle P(t_1)P(t_1+t_2)P(t_1+t_2+t_3)P(0)\rangle,\\
R_2(t_3,t_2,t_1)&\equiv\langle P(0)P(t_1+t_2)P(t_1+t_2+t_3)P(t_1)\rangle,\\
R_3(t_3,t_2,t_1)&\equiv\langle P(0)P(t_1)P(t_1+t_2)P(t_1+t_2+t_3)\rangle,\\
R_4(t_3,t_2,t_1)&\equiv\langle P(t_1+t_2+t_3)P(t_1+t_2)P(t_1)P(0)\rangle.
\end{aligned} \tag{10}$$

In Eqs. (10) $P(t)$ are Heisenberg operators whose time evolution is determined by the material Hamiltonian H, and the expectation values are taken with respect to the equilibrium density matrix of the system corresponding to the same Hamiltonian. These formal expressions will be evaluated in the coming sections.

III. EXCITON REPRESENTATION OF THE THIRD-ORDER RESPONSE

We shall be interested in the third-order optical response where only the ground, the one-exciton, and the two-exciton states of the electronic system are relevant. To recast the Hamiltonian using the exciton representation in the relevant vector space of states we introduce one-exciton and two-exciton creation (annihilation) operators $B_\mu^\dagger$ (B_μ) and $Y_{\bar\mu}^\dagger$ ($Y_{\bar\mu}$), respectively, with $\mu=1,\ldots N$ and $\bar\mu=1,\ldots, N(N-1)/2$, where N is the number of molecules in the aggregate. The exciton operators can be defined as

$$\begin{aligned}
B_\mu^\dagger|0\rangle&\equiv\sum_n \varphi_\mu(n)B_n^\dagger|0\rangle,\quad B_\mu^\dagger B_m^\dagger|0\rangle=0,\\
Y_{\bar\mu}^\dagger|0\rangle&\equiv\sum_{mn} \Psi_{\bar\mu}(m,n)B_m^\dagger B_n^\dagger|0\rangle,\quad Y_{\bar\mu}^\dagger B_m^\dagger|0\rangle=0,
\end{aligned} \tag{11}$$

where $|0\rangle$ is the electronic ground state. $\varphi_\mu(n)$ and $\Psi_{\bar\mu}(mn)$ represent the one-exciton and two-exciton eigenstates of the exciton Hamiltonian H_e with energies ϵ_μ and $\epsilon_{\bar\mu}$, respectively. In this representation two-exciton states are obtained by acting with two-exciton creation operators, which are bilinear combinations of one-exciton creation operators. Recasting the Hamiltonian in terms of exciton operators yields

$$H=H_0+H_1, \tag{12}$$

with

$$\begin{aligned}
H_0&\equiv\sum_\mu \epsilon_\mu B_\mu^\dagger B_\mu+\sum_{\bar\mu}\epsilon_{\bar\mu}Y_{\bar\mu}^\dagger Y_{\bar\mu}+\sum_\mu q_\mu^{(c)}B_\mu^\dagger B_\mu\\
&\quad+\sum_{\bar\mu} q_{\bar\mu}^{(c)}Y_{\bar\mu}^\dagger Y_{\bar\mu}+H_{\rm ph},\\
H_1&\equiv\sum_{\mu\nu}^{\mu\neq\nu} q_{\mu\nu}^{(c)}B_\mu^\dagger B_\nu+\sum_{\bar\mu\bar\nu}^{\bar\mu\neq\bar\nu} q_{\mu\nu}^{(c)}Y_{\bar\mu}^\dagger Y_{\bar\nu},
\end{aligned} \tag{13}$$

and the polarization operator P adopts the form

$$P=\sum_\mu d_\mu(B_\mu+B_\mu^\dagger)+\sum_{\mu\bar\mu} d_{\mu,\bar\mu}(Y_{\bar\mu}^\dagger B_\mu+B_\mu^\dagger Y_{\bar\mu}). \tag{14}$$

Expressions for the transition dipoles d_μ, $d_{\mu,\bar\mu}$ and the collective coordinates in the exciton representation $q_\mu^{(c)}$, $q_{\bar\mu}^{(c)}$, $q_{\mu\nu}^{(c)}$, and $q_{\bar\mu\bar\nu}^{(c)}$ in terms of the original collective coordinates $q_{mn}^{(c)}$ are given in Appendix A.

Using this representation, the correlation function F can be represented as a sum of two terms, which do not (F_1) and do (F_2) involve two-exciton states, in the sum-over-states expansion[1,22] of the r.h.s. of Eq. (9),

$$F(\tau_4,\tau_3,\tau_2,\tau_1)\equiv\sum_{j=1}^{2} F_j(\tau_4,\tau_3,\tau_2,\tau_1). \tag{15}$$

Equation (15) together with Eqs. (8)–(10) yield a sixteen term representation for the optical response function R

$$R(t_3,t_2,t_1)=\sum_{\alpha=1}^{4}\sum_{j=1}^{2}[R_{\alpha j}(t_3,t_2,t_1)-R^{*}_{\alpha j}(t_3,t_2,t_1)], \tag{16}$$

with

$$\begin{aligned}
R_{1j}(t_3,t_2,t_1)&=F_j(t_1,t_1+t_2,t_1+t_2+t_3,0),\\
R_{2j}(t_3,t_2,t_1)&=F_j(0,t_1+t_2,t_1+t_2+t_3,t_1),\\
R_{3j}(t_3,t_2,t_1)&=F_j(0,t_1,t_1+t_2+t_3,t_1+t_2),\\
R_{4j}(t_3,t_2,t_1)&=F_j(t_1+t_2+t_3,t_1+t_2,t_1,0).
\end{aligned} \tag{17}$$

Using the notation of section II, F_j can be represented in a form

$$F_1(\tau_4,\tau_3,\tau_2,\tau_1)=\sum_{\alpha\beta\mu\nu} d_\alpha d_\beta d_\nu d_\mu \langle B_\alpha(\tau_4)B^{\dagger}_\beta(\tau_3)B_\mu(\tau_2)B^{\dagger}_\nu(\tau_1)\rangle, \tag{18}$$

$$\begin{aligned}
F_2(\tau_4,\tau_3,\tau_2,\tau_1)&=\sum_{\alpha\beta\mu\nu}\sum_{\nu\mu} d_\alpha d_{\beta,\bar{\mu}} d_\nu d_{\mu,\bar{\nu}}\\
&\times\langle B_\alpha(\tau_4)B^{\dagger}_\beta(\tau_3)Y_{\bar{\mu}}(\tau_3)Y^{\dagger}_{\bar{\nu}}(\tau_2)B_\mu(\tau_2)B^{\dagger}_\nu(\tau_1)\rangle.
\end{aligned} \tag{19}$$

The response functions now represent a collection of four-level systems (the ground state, two one-exciton states and one two-exciton state, Fig. 1). The various collective bath coordinates q_μ, $q_{\bar{\mu}}$, $q_{\mu\nu}$, and $q_{\bar{\mu}\bar{\nu}}$ coupled to these electronic transitions are correlated.[47] The calculation simplifies considerably if H_1 in Eq. (12) can be neglected. This approximation is expected to hold for disordered aggregates, and will be justified in the next section. Neglecting H_1, the correlation functions F_j can be evaluated exactly, using the matrix of line broadening functions $g_{\mu\nu}(t)$, whose matrix elements are related to the spectral densities by[1]

$$\begin{aligned}
g_{\mu\nu}(t)\equiv&\int_{-\infty}^{\infty}\frac{d\omega}{2\pi}\frac{1-\cos(\omega t)}{\omega^2}\coth\left(\frac{\omega}{2T}\right)C_{\mu\nu}(\omega)\\
&+i\int_{-\infty}^{\infty}\frac{d\omega}{2\pi}\frac{\sin(\omega t)-\omega t}{\omega^2}C_{\mu\nu}(\omega).
\end{aligned} \tag{20}$$

The transformation from real-space to the exciton representation is given in Appendix A [see Eq. (A1) and definitions following Eq. (A3)]. The correlation functions given by Eqs. (18) and (19) can be evaluated using straightforward generalizations of the procedure presented in Ref. 1, which yields

$$\begin{aligned}
F_1(\tau_4,\tau_3,\tau_2,\tau_1)=&\sum_{\mu\nu} d_\mu^2 d_\nu^2\\
&\times\exp[-f^{(1)}_{\mu\nu}(\tau_4,\tau_3,\tau_2,\tau_1)\\
&-i\epsilon_\mu(\tau_2-\tau_1)-i\epsilon_\nu(\tau_4-\tau_3)],
\end{aligned} \tag{21}$$

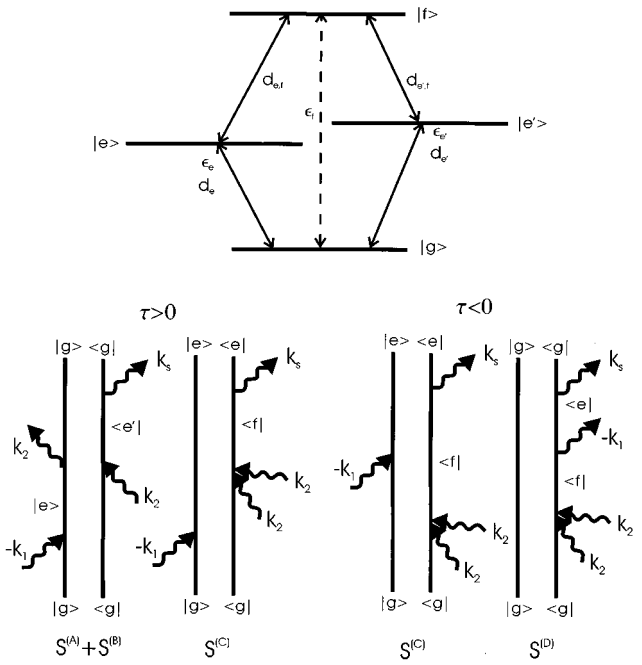

FIG. 1. Excitonic four-level system consisting a ground (g), two one-exciton (e,e'), and one two-exciton states (f). The third-order response of an aggregate is a sum of contributions from various collections of four-level systems. Bottom: The four double-sided Feynman-diagrams representing the time domain four-wave mixing [Eq. (34)].

$$\begin{aligned}
F_2(\tau_4,\tau_3,\tau_2,\tau_1)=&\sum_{\mu\nu\alpha} d_\mu d_\nu d_{\mu,\bar{\alpha}} d_{\nu,\bar{\alpha}}\\
&\times\exp[-f^{(2)}_{\mu\nu,\bar{\alpha}}(\tau_4,\tau_3,\tau_2,\tau_1)\\
&-i\epsilon_\mu(\tau_2-\tau_1)-i\epsilon_{\bar{\alpha}}(\tau_3-\tau_2)\\
&-i\epsilon_\nu(\tau_4-\tau_3)],
\end{aligned} \tag{22}$$

with

$$\begin{aligned}
f^{(1)}_{\mu\nu}(\tau_4,\tau_3,\tau_2,\tau_1)\equiv&g_{\mu\mu}(\tau_2-\tau_1)-g_{\mu\nu}(\tau_3-\tau_1)\\
&+g_{\mu\nu}(\tau_4-\tau_1)+g_{\mu\nu}(\tau_3-\tau_2)\\
&-g_{\mu\nu}(\tau_4-\tau_2)+g_{\mu\mu}(\tau_4-\tau_3),
\end{aligned} \tag{23}$$

$$\begin{aligned}
f^{(2)}_{\mu\nu,\bar{\alpha}}(\tau_4,\tau_3,\tau_2,\tau_1)\equiv&g_{\mu\mu}(\tau_2-\tau_1)-g_{\mu\bar{\alpha}}(\tau_2-\tau_1)\\
&+g_{\mu\bar{\alpha}}(\tau_3-\tau_1)-g_{\mu\nu}(\tau_3-\tau_1)\\
&+g_{\mu\nu}(\tau_4-\tau_1)-g_{\mu\bar{\alpha}}(\tau_3-\tau_2)\\
&+g_{\mu\nu}(\tau_3-\tau_2)-g_{\mu\nu}(\tau_4-\tau_2)\\
&+g_{\bar{\alpha}\bar{\alpha}}(\tau_3-\tau_2)-g_{\bar{\alpha}\nu}(\tau_3-\tau_2)\\
&+g_{\bar{\alpha}\nu}(\tau_4-\tau_2)-g_{\bar{\alpha}\nu}(\tau_4-\tau_3)\\
&+g_{\nu\nu}(\tau_4-\tau_3).
\end{aligned} \tag{24}$$

Equations (16)–(24) express the third-order response functions in terms of nuclear spectral densities convoluted with the various optical transitions. These results will be used in the numerical calculations presented in the coming sections.

IV. IMPULSIVE TWO-PULSE FOUR-WAVE-MIXING IN DISORDERED ONE-DIMENSIONAL AGGREGATES

We consider two-pulse four-wave mixing in self-diffraction geometry,[48,49] where the system is excited by two ultrashort pulses with wavevectors $\mathbf{k}_1$ and $\mathbf{k}_2$, and the signal is generated in the direction $\mathbf{2k}_2-\mathbf{k}_1$. We assume a model of a cyclic aggregate with nearest-neighbor intermolecular interactions. This model describes light-harvesting LH1 antenna complexes, as well as the B850 and B800 bands of LH2, which are highly symmetric circular one-dimensional aggregates with $N=32$, 18, and 9, respectively, as well as J-aggregates with linear structure (formally a linear aggregate can be obtained as a particular case of a cyclic aggregate by setting one nearest-neighbor coupling constant to zero).

For this model, the many-exciton states are represented by the Bethe Ansatz[50] and can be expressed in terms of two sets of one-exciton states: ordinary one-exciton states $\varphi_\mu(n)$ satisfying periodic boundary conditions $\varphi_\mu(n+N)=\varphi_\mu(n)$, and auxiliary one-exciton states $\overline{\varphi_\mu(n)}$ with antiperiodic boundary conditions $\overline{\varphi_\mu}(n+N)=-\overline{\varphi_\mu}(n)$, both being eigenstates of the one-exciton Hamiltonian with energies ϵ_μ and $\overline{\epsilon_\mu}$, respectively (see Appendix B).

The one- and the two-exciton states for the present model have the following form:

$$|\mu\rangle\equiv\sum_m \varphi_\mu(m)B_m^\dagger|0\rangle, \tag{25}$$

$$|\alpha\beta\rangle\equiv\sum_{mn} \epsilon_{mn}\overline{\varphi_\alpha}(m)\overline{\varphi_\beta}(n)B_m^\dagger B_n^\dagger|0\rangle, \tag{26}$$

where $\epsilon_{mn}=1,0,-1$ for $m<n$, $m=n$, and $m>n$, respectively, and in Eq. (26) $\alpha<\beta$. The states $|\mu\rangle$ and $|\overline{\alpha\beta}\rangle$ are normalized provided the functions $\varphi_\mu(n)$ and $\overline{\varphi_\mu}(n)$ are normalized. For simplicity we further assume diagonal coupling to the bath, i.e., $q_{mn}^{(c)}=\delta_{mn}q_n^{(c)}$, that all baths have the same spectral density and that the baths acting on different molecules are uncorrelated. This gives the following matrix of spectral densities

$$C_{mn,kl}(\omega)=\delta_{mn}\delta_{kl}\delta_{mk}C(\omega). \tag{27}$$

The Hamiltonians H_0 and H_1 representing the system-bath Hamiltonian (Eq. (12)) can be represented as

$$H_0=\sum_\alpha \epsilon_\alpha B_\alpha^\dagger B_\alpha+\sum_{\mu\nu}^{\mu<\nu}(\overline{\epsilon_\mu}+\overline{\epsilon_\nu})Y_{\mu\nu}^\dagger Y_{\mu\nu} +\sum_{\alpha n} g_{\alpha,n}B_\alpha^\dagger B_\alpha q_n^{(c)}+\sum_{\mu\nu n}^{\mu<\nu}\overline{g}_{\mu\nu,n}Y_{\mu\nu}^\dagger Y_{\mu\nu}q_n^{(c)}+H_{\rm ph}, \tag{28}$$

$$H_1=\sum_{\alpha\beta n}^{\alpha\neq\beta} g_{\alpha\beta,n}^{(1)}B_\alpha^\dagger B_\beta q_n^{(c)}+{\sum_{\mu\nu\nu' n}}' \overline{g}_{\mu\nu\nu',n}^{(1)}Y_{\mu\nu'}^\dagger Y_{\mu\nu}q_n^{(c)}, \tag{29}$$

where Σ' in Eq. (29) implies that a summation over μ, ν, and ν' under the condition that μ, ν, and ν' are all different, and

$$g_{\alpha n}\equiv|\varphi_\alpha(n)|^2,\quad \overline{g}_{\mu\nu,n}\equiv|\overline{\varphi_\mu}(n)|^2|\overline{\varphi_\nu}(n)|^2, \qquad g_{\alpha\beta,n}^{(1)}\equiv\varphi_\alpha(n)\varphi_\beta(n),\quad \overline{g}_{\mu\nu\nu',n}^{(1)}\equiv\varphi_{\nu'}(n)\varphi_\nu(n). \tag{30}$$

The polarization operator adopts a form

$$P=\sum_\alpha d_\alpha(B_\alpha+B_\alpha^\dagger)+\sum_{\alpha\mu\nu}^{\mu<\nu} d_{\alpha,\mu\nu}(Y_{\mu\nu}^\dagger B_\alpha+B_\alpha^\dagger Y_{\mu\nu}), \tag{31}$$

with

$$d_\alpha=\sum_m d_m\varphi_\alpha(m), \qquad d_{\alpha,\mu\nu}=\sum_{mn}\epsilon_{mn}\overline{\varphi_\mu}(m)\overline{\varphi_\nu}(n)[d_m\varphi_\alpha(n)+d_n\varphi_\alpha(m)]. \tag{32}$$

All relevant information about the bath is given by the spectral densities $C_{\mu\nu}(\omega)$, $C_{\overline{\mu\nu}}(\omega)$, $C_{\mu\overline{\nu}}(\omega)$, $C_{\mu,\alpha\beta}(\omega)$, $C_{\mu,\overline{\alpha\beta}}(\omega)$, $C_{\overline{\mu,\alpha\beta}}(\omega)$, $C_{\overline{\mu,\alpha\beta}}(\omega)$, $C_{\mu\nu,\alpha\beta}(\omega)$, $C_{\mu\nu,\overline{\alpha\beta}}(\omega)$, and $C_{\overline{\mu\nu,\alpha\beta}}(\omega)$, where the Greek indices $\alpha,\ldots$ represent symmetric one-exciton states and $\overline{\alpha},\ldots$ represent antisymmetric one-exciton states. The transformation relating these spectral densities to $C_{mn,kl}(\omega)$ is given in Appendix A.

We are now in a position to justify the neglect of H_1 in the derivation of Eqs. (20)–(24). Consider an aggregate with static disorder which leads to strong exciton localization: According to Mott, localized exciton states with close energies do not overlap spatially. One can see from Eq. (29) that only exciton states with overlapping wavefunctions interact through the bath. This implies that if two one- or two-exciton states interact, they must have a substantial energy difference, which is controlled by the Anderson localization length l_A. We can then treat H_1 as a small perturbation in aggregates with strong localization. In the zeroth approximation H_1 may be simply neglected. The only effect missed by neglecting H_1 is relaxation of exciton populations which can be taken into account using projection operator techniques by calculating a relaxation operator perturbatively in H_1. However, in the two-pulse measurements studied in this paper the system is prepared in an electronic coherence (rather than a population). The femtosecond signals are therefore not sensitive to exciton relaxation and we can safely neglect H_1. In the absence of static disorder one may not neglect the Hamiltonian H_1, since bath-induced interactions between excitons with close energies represented by H_1 are as important as bath-induced exciton self-interaction represented by the third and fourth terms in Eq. (28). This state of affairs can be formally described as follows. Let l_A be the exciton localization length in the aggregate if we switch off exciton-phonon coupling, whereas l_p is the polaron size (dynamical localization length) in our system in the absence of static disorder. Exciton self-trapping (polaron formation) in an ordered system is a self-interaction process, where the exciton is trapped

by lattice distortions, where the lattice distortion is caused by the presence of the exciton. Consider a system with static disorder and exciton-phonon coupling. If $l_A < l_p$ we can neglect effects of lattice distortion on exciton localization, i.e. the localization is primarily determined by static disorder. Our theory is therefore valid provided $l_p > l_A$, i.e. in the case of strong exciton localization which is believed to be the case in photosynthetic antenna complexes.[2,3,37] Due to repulsion of localized levels[51] off-diagonal exciton-phonon coupling terms with respect to the exciton basis set can be treated perturbatively, and the theory incorporates the spectral densities explicitly.

All expressions for the optical response given in the previous section apply to the general third-order response. Hereafter, we consider a two-pulse experiment, where the exciting field is given by

$$\begin{aligned} E(t) &= E_1(t)(e^{i\mathbf{k}_1\cdot\mathbf{r}-i\omega_1 t}+e^{-i\mathbf{k}_1\cdot\mathbf{r}+i\omega_1 t}) \\ &\quad + E_2(t)(e^{i\mathbf{k}_2\cdot\mathbf{r}-i\omega_2 t}+e^{-i\mathbf{k}_2\cdot\mathbf{r}+i\omega_2 t}) \\ &\equiv E_1^+(t)e^{-i\omega_1 t}+E_1^-(t)e^{i\omega_1 t}+E_2^+(t)e^{-i\omega_2 t} \\ &\quad + E_2^-(t)e^{i\omega_2 t}. \end{aligned} \tag{33}$$

Here, $E_{1,2}(t)$ are the pulse envelopes. The terms E_i^+ (E_i^-) refer to the components of E with directions $+\mathbf{k}_i$ $(-\mathbf{k}_i)$. This field will create excitations associated with different directions $e^{i\mathbf{k}_s\cdot\mathbf{r}}$, $\mathbf{k}_s = n\mathbf{k}_1 + m\mathbf{k}_2$, where n,m can be any integers.[52–54] While decomposing the signal with respect to the directions, we also invoke the rotating-wave approximation (RWA). This can be done easily, since the directions $+\mathbf{k}_i$ $(+\mathbf{k}_i)$ are associated with a negative (positive) central laser frequencies $-\omega_i$ $(+\omega_i)$. Within the RWA we only retain the resonant terms for each interaction. This approximation is well justified for a resonant excitation, i.e. $\omega_1 \approx \omega_2 \approx \epsilon_\alpha$, where ϵ_α refers to the frequency of a one-exciton state, and for excitations with laser pulses whose pulsewidths ($\hat{E}_1$, $\hat{E}_2$) are longer than the inverse of the optical (band-gap) frequencies, i.e. $\hat{E}_1, \hat{E}_2 \gg \omega_1^{-1}, \omega_2^{-1}, \epsilon_\alpha^{-1}$. Even for the short 35 fs laser pulses used in Ref. 18 the RWA is well justified.

In the following we consider two-pulse four-wave mixing experiments where the signal is emitted in the direction $\mathbf{k}_s = 2\mathbf{k}_2 - \mathbf{k}_1$. The two-pulse four-wave-mixing signal in the impulsive excitation limit is characterized by two times: the time delay τ between the two pulses and the time of observation t. We make the following choice of time variables: pulse 2 comes at time 0, and pulse 1 at time $-\tau$. The polarization at time t will be denoted $S_0(t,\tau)$. A positive (negative) τ implies that pulse 1 arrives before (after) pulse 2. Note that, unlike τ, the time arguments of the response function R are positive and represent the time-intervals between successive interactions with the pulses. For short pulses (the snapshot limit), i.e., for $E_1^+(t) = E_1^+ e^{i\mathbf{k}_1\cdot\mathbf{r}}\delta(t+\tau)$, $E_1^-(t) = E_1^- e^{-i\mathbf{k}_1\cdot\mathbf{r}}\delta(t+\tau)$, $E_2^+(t) = E_2^+ e^{i\mathbf{k}_2\cdot\mathbf{r}}\delta(t)$, and $E_2^-(t) = E_2^- e^{-i\mathbf{k}_2\cdot\mathbf{r}}\delta(t)$ (although here $E_i^- = E_i^+$ we retain our notation which keeps track of the directions). Within the RWA the time-resolved third-order polarization in the direction $\mathbf{k}_s = 2\mathbf{k}_2 - \mathbf{k}_1$ adopts the form [cp. Eq. (7)]:

$$\begin{aligned} S_0(t,\tau) &= i^3 E_1^-(E_2^+)^2(\Theta(\tau)R(t,0,\tau) \\ &\quad + \Theta(-\tau)R(t+\tau,-\tau,0)). \end{aligned} \tag{34}$$

The time-resolved polarization is a complex valued function given by either its real or imaginary parts or by its amplitude and phase

$$S_0(t,\tau) = |S_0(t,\tau)|e^{i\varphi(t,\tau)-i\tilde{\omega}(t-\tau)}, \tag{35}$$

where $\tilde{\omega}$ is an arbitrary reference frequency, which defines a rotating frame. If $\tilde{\omega}$ is close to the exciton energies ϵ_α it suppresses the fast rotation with optical frequencies and leads to a slowly varying $\varphi(t,\tau)$. The polarization in the frequency-domain is given by

$$S_0(\omega,\tau) = \int S_0(t,\tau)e^{i\omega t}\,dt. \tag{36}$$

Heterodyne detection involves mixing the FWM polarization with an additional heterodyne field $E_{\rm het}$

$$E_{\rm het}(t) = \mathscr{E}_{\rm het}(t-t_0)e^{-i\tilde{\omega}t+i\mathbf{k}_s\cdot\mathbf{r}} + \text{c.c.}, \tag{37}$$

and the resulting signal is

$$S_{\rm het}(t,\tau,\tilde{\omega}) = \mathrm{Im}\left[\int_{-\infty}^{\infty} dt\; E_{\rm het}^*(t-t_0)S_0(t,\tau)\right]. \tag{38}$$

Using an ultrashort heterodyning pulse, i.e., $E_{\rm het}(t) = \mathscr{E}_{\rm het}\delta(t-t_0)$, we have the time-resolved detection $S_{\rm het}(t_0,\tau) = \mathrm{Im}[\mathscr{E}_{\rm het}^* S_0(t_0,\tau)]$. By varying the phase and the temporal position of $\mathscr{E}_{\rm het}$ the total information contained in $S_0(t,\tau)$ can be recovered.[48] In the opposite limit $E_{\rm het}(t) = \mathscr{E}_{\rm het}e^{-i\tilde{\omega}t}$ we have the frequency-resolved detection $S_{\rm het}(\tilde{\omega},\tau) = \mathrm{Im}[\mathscr{E}_{\rm het}^*(\tilde{\omega})S_0(\tilde{\omega},\tau)]$. To obtain this information experimentally the signal field mixed with the heterodyne field $E_{\rm het}^*(t)S_0(t,\tau)$ is spectrally resolved.[55]

The complex-valued time-resolved signal field may be conveniently displayed using its Wigner-spectrogram (WS) defined by

$$S_{\rm WS}(t,\omega,\tau) = \int_{-\infty}^{\infty} S_0^*\left(t-\frac{t'}{2},\tau\right)S_0\left(t+\frac{t'}{2},\tau\right)e^{i\omega t'}\,dt'. \tag{39}$$

The WS is by definition a real quantity which depends on the observation time, the frequency, and on the time-delay. Upon integrating the WS over time (frequency) we obtain the amplitudes of the ordinary frequency-resolved (time-resolved) FWM signals[56]

$$|S_0(\omega,\tau)|^2 = \int_{-\infty}^{\infty} S_{\rm WS}(t,\omega,\tau)dt, \tag{40}$$

$$|S_0(t,\tau)|^2 = \int_{-\infty}^{\infty} S_{\rm WS}(t,\omega,\tau)d\omega. \tag{41}$$

The WS can be easily constructed from experiments[48,55] in which both the amplitude and the phase of the signal field are measured.

Experimentally the time- and frequency-domain amplitudes are obtained with a finite resolution determined by a gating function Φ.[57] For a time gating

$$S_{\mathrm{TG}}(t,\tau)=\int_{-\infty}^{\infty}dt'|S_0(t',\tau)|^2|\Phi(t-t')|^2. \tag{42}$$

A constant time-independent time-gating function corresponds to the time-integrated detection

$$S_{\mathrm{INT}}(\tau)=\int_{-\infty}^{\infty}|S_0(t,\tau)|^2\,dt. \tag{43}$$

For frequency-gating we have

$$S_{\mathrm{FG}}(\omega,\tau)=\int_{-\infty}^{\infty}d\omega'|S_0(\omega',\tau)|^2|\Phi(\omega-\omega')|^2. \tag{44}$$

In the exciton representation, the time-resolved polarization can be expressed as

$$S_0(t,\tau)=S^{(1)}(t,\tau)+S^{(2)}(t,\tau), \tag{45}$$

$$\begin{aligned}S^{(1)}(t,\tau)=&\,i^3E_1^-(E_2^+)^2\Theta(t)\Theta(\tau)\sum_{\alpha\beta}2|d_\alpha|^2|d_\beta|^2\\&\times\exp[-i(\epsilon_\beta t-\epsilon_\alpha\tau)]f^{(1)}_{\alpha,\beta}(t,\tau),\end{aligned} \tag{46}$$

$$\begin{aligned}S^{(2)}(t,\tau)=&-i^3E_1^-(E_2^+)^2\sum_{\alpha\mu\nu}^{\mu\neq\nu}d_\alpha d^{(2)}_{\mu\nu}d_{\alpha,\mu\nu}[(\Theta(t)\Theta(\tau)\\&+\Theta(t+\tau)\Theta(-\tau))\\&\times\exp[-i[(\overline{\epsilon_\mu}+\overline{\epsilon_\nu}-\epsilon_\alpha)t-\epsilon_\alpha\tau]]f^{(2)}_{\alpha,\mu\nu}(t,\tau)\\&-\Theta(t+\tau)\Theta(-\tau)\exp[-i[\epsilon_\alpha t\\&-(\overline{\epsilon_\mu}+\overline{\epsilon_\nu}-\epsilon_\alpha)\tau]]f^{(2)}_{\alpha,\mu\nu}(-\tau,-t)],\end{aligned} \tag{47}$$

where

$$d^{(2)}_{\mu\nu}\equiv\sum_{mn}\epsilon_{mn}\overline{\varphi_\mu}(m)\,\overline{\varphi_\nu}(n)d_nd_n, \tag{48}$$

and

$$\begin{aligned}f^{(1)}_{\alpha,\beta}(t,\tau)\equiv&\exp[-\overline{f^{(1)}_{\alpha,\beta}}(t,\tau)],\\f^{(2)}_{\alpha,\mu\nu}(t,\tau)\equiv&\exp[-\overline{f^{(2)}_{\alpha,\mu\nu}}(t,\tau)],\end{aligned} \tag{49}$$

$$\begin{aligned}\overline{f^{(1)}_{\alpha,\beta}}(t,\tau)=&(C_{\alpha\alpha}+C_{\alpha\beta})g^*(\tau)+C_{\beta\beta}g(t)+C_{\alpha\beta}g^*(t)\\&-C_{\alpha\beta}g^*(t+\tau),\end{aligned} \tag{50}$$

$$\begin{aligned}\overline{f^{(2)}_{\alpha,\mu\nu}}(t,\tau)=&C^{(1)}_{\alpha,\mu\nu}g^*(\tau)+(C^{(2)}_{\mu\nu,\mu\nu}-C^{(1)}_{\alpha,\mu\nu})g(t)\\&+(C_{\alpha\alpha}-C^{(1)}_{\alpha,\mu\nu})g^*(t+\tau)\end{aligned} \tag{51}$$

and

$$\begin{aligned}C_{\alpha\beta}\equiv&\sum_n|\varphi_\alpha(n)\varphi_\beta(n)|^2,\\C^{(1)}_{\alpha,\mu\nu}\equiv&\sum_n|\varphi_\alpha(n)|^2[|\overline{\varphi_\mu}(n)|^2+|\overline{\varphi_\nu}(n)|^2],\end{aligned} \tag{52}$$

$$\begin{aligned}C^{(2)}_{\mu'\nu',\mu\nu}\equiv&\sum_n[|\overline{\varphi_{\mu'}}(n)|^2+|\overline{\varphi_{\nu'}}(n)|^2]\\&\times[|\overline{\varphi_\mu}(n)|^2+|\overline{\varphi_\nu}(n)|^2].\end{aligned} \tag{53}$$

The contribution $S^{(1)}$ is related to correlations of one-exciton states, whereas $S^{(2)}$ reflects correlations between one- and two-exciton states. We shall partition $S^{(1)}\equiv S^{(A)}+S^{(B)}$, where $S^{(A)}$ includes the terms with $\alpha=\beta$, whereas $S^{(B)}$ is the sum over the terms with $\alpha\neq\beta$ in the r.h.s. of Eq. (46). We further partition $S^{(2)}\equiv S^{(C)}+S^{(D)}$ where $S^{(C)}$ is given by the first two lines of Eq. (47) and $S^{(D)}$ refers to the term in last line. We finally obtain (see double sided Feynman-diagrams displayed in Fig. 1)

$$S_0(t,\tau)=S^{(A)}(t,\tau)+S^{(B)}(t,\tau)+S^{(C)}(t,\tau)+S^{(D)}(t,\tau). \tag{54}$$

$S^{(A)}$ represents exciton self-correlation and is formally equivalent to a signal from a set of non-interacting two-level systems, $S^{(B)}$ describes correlations between pairs of single exciton states, whereas $S^{(C)}$ and $S^{(D)}$ originates from correlations between one- and two-exciton states. For positive time delays the single-exciton contributions $S^{(A)}$ and $S^{(B)}$, and the two-exciton contribution $S^{(C)}$ are non-zero. For negative time delay only the two contributions involving two-excitons $S^{(C)}$ and $S^{(D)}$ are non-zero.

V. INTERPLAY OF ONE- AND TWO-EXCITON DYNAMICS

The third-order polarization given by Eqs. (45)–(47) is expressed as a sum over contributions from various excitonic four-level systems (see Fig. 1), consisting of the ground, two one-exciton, and one two-exciton states. To analyze the signatures of the various physical processes on the FWM signal, we study in this section a series of simplified two-, three-, and four-level models, which give physical insight into the single-exciton and two-exciton dynamics associated with each time interval and how they can be detected by different measurements.

In the following calculations we assume an explicit form of $g(t)$ corresponding to the overdamped Brownian oscillator model, which depends on an exciton-phonon coupling strength λ, and a nuclear relaxation rate Λ. For this model $g(t)$ can be calculated analytically,[1] and the formula includes a summation over all Matsubara frequencies $2\pi nk_BT/\hbar$, $n=1,\ldots$. Even though it would be possible to perform the calculations presented in this section with the complete expression for $g(t)$, we restrict our analysis to the high temperature limit $k_BT\gg\hbar\Lambda$, in which $g(t)$ is given by[1]

$$g(t)=\left(\frac{2\lambda k_BT}{\hbar\Lambda^2}-i\frac{\lambda}{\Lambda}\right)[\exp(-\Lambda t)+\Lambda t-1]. \tag{55}$$

The real part of $g(t)$ describes the decay of optical excitations, whereas the imaginary part represents renormalizations of the transition frequencies induced by nuclear dynamics (the Stokes shift). If the nuclear relaxation rate Λ is small compared to the effective exciton-phonon coupling strength

($\sqrt{2\lambda k_B T}$), the exponential in Eq. (55) can be expanded in a Taylor series, resulting in a short-time approximation of $g(t) \propto t^2$.[1] In the opposite extreme (large Λ), the $\exp(-\Lambda t)$ term vanishes rapidly and may be ignored, and furthermore, at long times the 1 is smaller than Λt, and may also be neglected. This results in $g(t)=[(2\lambda k_B T/\hbar\Lambda^2)-i(\lambda/\Lambda)]\Lambda t$,[1] which corresponds to a time-independent renormalization of the transition frequency given by half the Stokes shift (λ) and homogeneous dephasing, i.e., a single exponential decay of the optical coherence. The third-order polarization for this model is given in Appendix C.

We start by assuming that only a single one-exciton state (with frequency ϵ_1) is relevant, i.e. the excitonic system is represented by a two-level model. Under this assumption the summations over α and m in Eq. (C1) reduce to the terms with $\alpha=m=1$. We note that since only one-exciton states are involved, due to the $\Theta(\tau)$ function in $a_{11}(t,\tau)$ [see Eq. (C3)], the FWM signal within the RWA only shows up for positive time delays. Without invoking the RWA we would have a very small signal for negative τ. Apart from the Θ-functions contained in $a_{11}(t,\tau)$, the time dependence of the terms appearing in Eq. (C1) is given by $\exp[-i(\epsilon_{11}^{(1)}t-\epsilon_{11}^{(2)}\tau)]\exp[-(n_2-n_3)\Lambda t-(n_1+n_2)\Lambda\tau]$. In the homogeneous limit the time dependence becomes simply $\exp[-i\epsilon_1(t-\tau)]\exp[-(C_{11}(2\lambda k_B T/\hbar\Lambda^2)-i(\lambda/\Lambda))(\Lambda t)]$. The time-resolved FWM amplitude then has a maximum at $t=0$ (note that the origin of t is right after pulse 2 has excited the system). It subsequently decays single exponentially with time constant $\Gamma^{-1}=1/(2\lambda k_B T/\hbar\Lambda)$, showing the usual free-induction decay of a two-level system[58]

$$S_0(t,\tau)\propto\Theta(t)\Theta(\tau)d_1^4 e^{-i\tilde{\epsilon}_1(t-\tau)}e^{-\Gamma(t+\tau)}. \tag{56}$$

The optical frequency of the complex signal is given by $\tilde{\epsilon}_1=\epsilon_1-C_{11}\lambda$. Transforming into a rotating frame eliminates this frequency. In this frame the phase of the FWM polarization shows no dynamics; this is to be expected, since the signal is characterized by a single frequency, and neither excitonic-induced nor nuclear-induced frequency changes are considered in the present model. The frequency-domain signal has therefore a simple Lorentzian line shape with a single resonance at $\omega=\tilde{\epsilon}_1$. The time-integrated FWM signal can be calculated analytically and is given by the integral over the square of the amplitude [see Eq. (43)].[58] It is characterized as a single exponential decay with a time constant $1/(2\Gamma)$, where the factor 2 accounts for the definition of the time-integrated signal. The WS for this model reads

$$S_{\mathrm{WS}}(t,\tau,\omega)\propto\Theta(\tau)\Theta(t)\exp(-2\Gamma(t+\tau))\times\frac{\sin(2(\tilde{\epsilon}_1-\omega)t)}{\tilde{\epsilon}_1-\omega}. \tag{57}$$

For the present model the FWM signal as well as its WS vanish for negative τ. At short t, S_{WS} grows linearly in t, for intermediate $t\approx\Gamma^{-1}$ it reaches a maximum, and for large t and τ decays exponentially with a time constant $(2\Gamma)^{-1}$. Furthermore the WS is a symmetric function of frequency around $\omega=\tilde{\epsilon}_1$. This symmetry, which is also present in the power spectrum [the amplitude of the frequency domain signal, see Eq. (36)], is a direct consequence of the absence of any non-trivial dynamics of the phase.[59] It oscillates as function of ω for positive and negative values, and the ''oscillation frequency'' decreases with increasing time, which demonstrates that only resonant excitations survive at long times; this behavior reflects the build-up of energy conservation, as shown in standard derivations of Fermi's golden rule.

We next analyze the effects of disorder on the two-level model. The simplest way to include disorder is by averaging the signal over a distribution of transition frequencies, i.e. adding inhomogeneous broadening of the transition frequency. Assuming a Gaussian distribution

$$f_1(\epsilon_1)=\exp(-((\epsilon_1-\hat{\epsilon}_1)/\overline{\epsilon_1})^2), \tag{58}$$

and performing the integration

$$S_0(t,\tau)=\int_{-\infty}^{\infty} S_0^{\tilde{\epsilon}_1}(t,\tau)f_1(\tilde{\epsilon}_1)d\tilde{\epsilon}_1 \tag{59}$$

results in the FWM polarization

$$S_0(t,\tau)\propto\Theta(t)\Theta(\tau)e^{-i\hat{\epsilon}_1(t-\tau)}e^{-((t-\tau)\overline{\epsilon_1}/2)^2}e^{-\Gamma(t+\tau)}. \tag{60}$$

For small Γ the signal given by Eq. (60) is emitted as a photon echo,[58] i.e., the time-resolved polarization has a maximum at $t=\tau$, concomitantly, also the maximum of the WS is not determined by the dephasing rate Γ but appears close to $t\approx\tau$. For larger Γ comparable to the width of the inhomogeneous distribution function $\overline{\epsilon_1}$, the signal will have a maximum at earlier times $t<\tau$.

Another interesting case is the limit of slow nuclear dynamics, which for short times results in $g(t)=\lambda k_B T t^2/\hbar$. In this limit $g(t)$ is real, i.e. leads to no nuclear-induced renormalization of the transition frequency, and merely describes dephasing of the optical excitations. The time-resolved FWM polarization is then

$$S_0(t,\tau)\propto\Theta(t)\Theta(\tau)e^{-i\epsilon_1(t-\tau)}e^{-C_{11}\lambda k_B T(t^2+\tau^2)/\hbar}. \tag{61}$$

Except for the replacement of the exponential used in the homogeneous limit by a Gaussian, all other statements concerning the absence of dynamics of the phase, the symmetry of the WS, and the buildup of a photon echo for an inhomogeneously broadened system given above remain valid in this limit.

Evaluation of the full formula given by Eq. (C1) including the summations over n_1, n_2, and n_3 should allow us to interpolate between these two extreme cases, which are characterized by exponential and Gaussian correlation functions. A numerical evaluation of Eq. (C1) would be easily feasible since for large n_1, n_2, and n_3 the magnitude of the terms decreases very quickly due to the factorials in the denominators. The terms appearing for large n_1, n_2, and n_3 represent fast decaying contributions as function of t and τ, which in the frequency-domain represent very broad lines with widths $n_i\Gamma$.

We next turn to a three-level system made of the ground state and two one-exciton states with frequencies ϵ_1 and ϵ_2, respectively. The time-resolved FWM signal in the homogeneous limit assuming a single Γ is then given by

$$S_0(t,\tau)\propto\Theta(t)\Theta(\tau)[d_1^4 e^{-i\tilde{\epsilon}_1(t-\tau)}+d_2^4 e^{-i\tilde{\epsilon}_2(t-\tau)} + d_1^2 d_2^2(e^{-i(\tilde{\epsilon}_1 t-\tilde{\epsilon}_2\tau)}+e^{-i(\tilde{\epsilon}_2 t-\tilde{\epsilon}_1\tau)})]e^{-\Gamma(t+\tau)}. \tag{62}$$

The first two terms on the r.h.s. of Eq. (62) represent the two two-level contributions of the two one-exciton states discussed above, and the last two terms represent interference terms which arise since the two optical transitions share a common (ground) state. We thus have a genuine quantum-beat system (and not a polarization interference system which consists of two uncoupled transitions, compare discussion in Refs. 1,49,60). Since only one-exciton states are considered, the signals are finite only for positive τ. As for the two-level system, the temporal envelope of the amplitude shows an exponential decay with rate Γ. If Γ is not larger than $\tilde{\epsilon}_1-\tilde{\epsilon}_2$ and the transition dipoles d_1 and d_2 are comparable it is modulated as function of t and τ as $\cos((\tilde{\epsilon}_1-\tilde{\epsilon}_2)t)\cos((\tilde{\epsilon}_1-\tilde{\epsilon}_2)\tau)$, i.e., shows oscillation with the energy difference the single and two-exciton states. Therefore the phase of the signal will also show an oscillatory pattern with respect to a reference frequency chosen in between the two exciton transition frequencies. If the transition dipoles d_1 and d_2 are comparable and Γ is not too large, the frequency-domain signal has two-resonances. The amplitudes of these resonances vary with the time delay as $\cos((\tilde{\epsilon}_1-\tilde{\epsilon}_2)\tau)$.[60] The WS for the three-level system is then given by

$$S_{\mathrm{WS}}(t,\tau,\omega)\propto\Theta(\tau)\Theta(t)\exp[-2\Gamma(t+\tau)] \times\sum_{\alpha\beta\gamma\delta=1}^{2} d_\alpha^2 d_\beta^2 d_\gamma^2 d_\delta^2 e^{i(\tilde{\epsilon}_\delta-\tilde{\epsilon}_\beta)\tau}e^{-i(\tilde{\epsilon}_\alpha-\tilde{\epsilon}_\gamma)t} \times\frac{\sin(2(\tilde{\epsilon}_{\alpha\gamma}-\omega)t)}{\tilde{\epsilon}_{\alpha\gamma}-\omega}, \tag{63}$$

with $\tilde{\epsilon}_{\alpha\gamma}=(\tilde{\epsilon}_\alpha+\tilde{\epsilon}_\gamma)/2$. The WS may have resonances at $\omega=\tilde{\epsilon}_1$, $\tilde{\epsilon}_2$, and $(\tilde{\epsilon}_1+\tilde{\epsilon}_2)/2$. If $d_1=d_2$, the WS and the power spectrum are symmetric functions of frequency around $\omega=(\tilde{\epsilon}_1+\tilde{\epsilon}_2)/2$, whereas if $d_1\neq d_2$ the phase dynamics will introduce some asymmetry.

A simple way to include disorder effects for the three-level system is again to assume that the disorder does not influence the exciton-phonon coupling, but introduces an inhomogeneous distribution of the two transition frequencies $f(\epsilon_1,\epsilon_2)$. While for the two-level model the distribution function depends only on a single variable ϵ_1 (which may lead to echoes in the time-resolved polarization) this is more involved for the three-level system, since two transition frequencies need to be considered. The simplest case assumes a completely correlated Gaussian disorder

$$f_2(\epsilon_1,\epsilon_2)=\delta(\epsilon_1-\epsilon_2+\Delta)\exp(-((\epsilon_1-\hat{\epsilon}_1)/\overline{\epsilon_1})^2). \tag{64}$$

As in the two-level case, introducing such an inhomogeneous broadening via

$$S_0(t,\tau)=\int_{-\infty}^{\infty}\int_{-\infty}^{\infty} S_0^{\tilde{\epsilon}_1\tilde{\epsilon}_2}(t,\tau)f_2(\tilde{\epsilon}_1,\tilde{\epsilon}_2)d\tilde{\epsilon}_1\, d\tilde{\epsilon}_2, \tag{65}$$

gives for the time-resolved polarization [denoting $\hat{\epsilon}_2=\hat{\epsilon}_1+\Delta$, see Eq. (64)]

$$S_0(t,\tau)\propto\Theta(t)\Theta(\tau)e^{-((t-\tau)\overline{\epsilon_1}/2)^2}[d_1^4 e^{-i\hat{\epsilon}_1(t-\tau)} + d_2^4 e^{-i\hat{\epsilon}_2(t-\tau)}+d_1^2 d_2^2(e^{-i(\hat{\epsilon}_1 t-\hat{\epsilon}_2\tau)} + e^{-i(\hat{\epsilon}_2 t-\hat{\epsilon}_1\tau)})]e^{-\Gamma(t+\tau)}. \tag{66}$$

For correlated disorder, the three-level signal also is emitted as a photon-echo with an maximum at $t=\tau$.

Other examples for possible distribution functions include a completely anti-correlated disorder, i.e.,

$$f_2(\epsilon_1,\epsilon_2)=\delta(\epsilon_1+\epsilon_2+\Delta)\exp(-((\epsilon_1-\hat{\epsilon}_1)/\overline{\epsilon_1})^2), \tag{67}$$

or an uncorrelated disorder, i.e.,

$$f_2(\epsilon_1,\epsilon_2)=\exp(-((\epsilon_1-\hat{\epsilon}_1)/\overline{\epsilon_1})^2) \times\exp(-((\epsilon_2-\hat{\epsilon}_2)/\overline{\epsilon_2})^2). \tag{68}$$

For both cases described by Eqs. (67) and (68), different factors appear instead of $e^{-((t-\tau)\overline{\epsilon_1}/2)^2}$ in front of the four terms on the r.h.s. of Eq. (66). While the first two terms involving only a single exciton state show photon-echoes, the latter two decay rapidly, due to the absence of any correlation between the two frequencies. This implies that regardless of the degree of correlation of the disorder, the terms involving a single exciton (A) are always photon echo-like, while the terms involving two one-exciton states (B) generate photon-echoes only if the disorder is correlated.

Finally we consider a four-level system consisting of the ground, two one-exciton, and one two-exciton state, see Fig. 1. The total signal [Eqs. (45) and (C1)] can be written as a sum over four-level contributions. In this case the time-resolved polarization in the homogeneous limit (assuming a single dephasing rate Γ for the optical transitions and 2Γ for the coherences between ground and two-exciton states is given by [compare with Eqs. (C1)–(C4)]

$$S_0(t,\tau)\propto\Theta(t)\Theta(\tau)[d_1^4 e^{-i\tilde{\epsilon}_1(t-\tau)}+d_2^4 e^{-i\tilde{\epsilon}_2(t-\tau)} + d_1^2 d_2^2(e^{-i(\tilde{\epsilon}_1 t-\tilde{\epsilon}_2\tau)}+e^{-i(\tilde{\epsilon}_2 t-\tilde{\epsilon}_1\tau)})]e^{-\Gamma(t+\tau)} - \frac{1}{2}\sum_{\alpha=1}^{2} d_\alpha d^{(2)}_{\mu(N+1)\nu(N+1)}d_{\alpha,\mu(N+1)\nu(N+1)} \times e^{-\Gamma(t+|\tau|)}((\Theta(t)\Theta(\tau)+\Theta(t+\tau)\Theta(-\tau)) \times e^{-i(\epsilon^\alpha_{N+1}t-\tilde{\epsilon}_\alpha\tau)}-\Theta(t+\tau)\Theta(-\tau) \times e^{-i(\tilde{\epsilon}_\alpha t-\epsilon^\alpha_{N+1}\tau)}). \tag{69}$$

Compared to the three-level case, two new frequencies ϵ^α_{N+1} appear, which describe the transitions between one- and two-exciton states and may lead to additional resonances and

modulations in the frequency- and time-domain signals, respectively. The presence of two-exciton states leads to finite signals also for negative time delays, which are absent if only one-exciton states are considered. It should be noted that the two-exciton contributions appearing for positive time delay have a different sign compared to the one-exciton contributions [see $-$ sign in front of the third line in Eq. (69)]. This sign-change introduces strong cancellations between one-exciton and two-exciton contributions to the FWM signal and its significance will be illustrated in the next section where the two-pulse FWM signals of LH2 will be calculated. For negative time delays there are two terms involving two-excitons (see Feynman diagrams, Fig. 1), which have different signs and therefore partially cancel. As in the three-level case, the two-exciton contributions to the FWM signals also depend on the degree of correlation present in the disorder, which can in this case be expressed by a distribution function $f_3(\epsilon_1,\epsilon_2,\epsilon_3)$ where ϵ_3 refers to the frequency of the two exciton state. The correlations present in f_3 determine whether the time-resolved FWM signal is emitted as a photon-echo or simply decays rapidly (free induction decay) once disorder is incorporated. In the numerical investigations presented in the next section we include different models of disorder for the molecular transitions frequencies and calculate for each realization of disorder both one- and two-exciton states. Therefore there is a strong correlation between the disorder-induced frequency distributions associated with one- and two-exciton states, which can be expressed as

$$f_3(\epsilon_1,\epsilon_2,\epsilon_3)=f_2(\epsilon_1,\epsilon_2)\,\delta(\epsilon_3-g(\epsilon_1,\epsilon_2)), \tag{70}$$

indicating that the frequency of the two-exciton state (ϵ_3) is uniquely determined by the one-exciton frequencies ϵ_1 and ϵ_2. If for example due to disorder with a long correlation length (model IV, see Sec. VI), both ϵ_1 and ϵ_2 are changed by $\delta\omega$, ϵ_3 will change by $2\,\delta\omega$.

VI. NUMERICAL STUDY OF TWO-PULSE FOUR-WAVE MIXING IN LH2

To analyze the combined effects of disorder and exciton-phonon coupling characterized by the nuclear spectral density, we have performed a series of five model calculations. In models I-III we use spectral densities of different forms and static disorder. Model IV has a spectral density together with inhomogeneous broadening, whereas model V has homogeneous dephasing with static disorder. In models I, II, and III, we have included disorder with a short correlation length, introduced by assuming independent Gaussian distributions with full width at half maximum (FWHM) σ [$\sigma=2\sqrt{\ln 2}\,\overline{\epsilon_1}$, see Eq. (58)] for each molecular frequency (the Anderson model), and chose different spectral densities

$$C_{\rm I}(\omega)=2\lambda\,\frac{\omega\tau_1}{\omega^2\tau_1^2+1}, \tag{71}$$

$$C_{\rm II}(\omega)=\lambda\,\omega\sqrt{\pi}\,\tau_2\exp\left(-\frac{\omega^2\tau_2^2}{4}\right), \tag{72}$$

$$C_{\rm III}(\omega)=\frac{\lambda}{2}\left[\frac{i\omega\tau_3 e^{i\phi_3}}{(\omega+\omega_3)\tau_3+i}-\frac{i\omega\tau_3 e^{-i\phi_3}}{(\omega-\omega_3)\tau_3-i}+\text{c.c.}\right]. \tag{73}$$

In the high temperature limit ($\beta\hbar\omega\ll 1$) the spectral broadening function $g(t)$ may be recast in the form

$$g(t)=\frac{2\lambda k_B T}{\hbar}\int_0^t dt_2\int_0^{t_2} dt_1\; M(t_1) - i\lambda\int_0^t dt_1[1-M(t_1)], \tag{74}$$

where $M(t)$ is related to the spectral density $C(\omega)$ by[1]

$$M(t)=\frac{1}{\pi\lambda}\int_0^\infty d\omega\,\frac{C(\omega)}{\omega}\cos(\omega t), \tag{75}$$

and 2λ is the Stokes shift, with

$$\lambda=\frac{1}{\pi}\int_0^\infty d\omega\,\frac{C(\omega)}{\omega}. \tag{76}$$

Inverting Eq. (75) gives

$$C(\omega)=\lambda\,\omega\int_{-\infty}^{\infty} dt\; e^{i\omega t}M(t). \tag{77}$$

$M(t)$ is the transition frequency correlation function which is directly observed in time-resolved Stokes-shift measurements. For models I, II and III we thus have

$$M_I(t)=e^{-|t|/\tau_1}, \tag{78}$$

$$M_{II}(t)=e^{-(t/\tau_2)^2}, \tag{79}$$

$$M_{III}(t)=e^{-|t|/\tau_3}\cos(\omega_3|t|+\phi_3). \tag{80}$$

Model I is the overdamped Brownian oscillator studied in Sec. V [comparing Eq. (78) to Eq. (55) we have used $\tau_1=\Lambda^{-1}$].

The relaxation times associated with these correlation functions were taken from Ref. 18 where experimental results on three-pulse four-wave mixing have been fitted assuming that $M(t)$ is given by a sum of 7 contributions. For the exponential (model I) we used $\tau_1=130$ fs, for the Gaussian (model II) $\tau_2=40$ fs, and for the cosine (model III) a frequency of $\omega_3=190\ \text{cm}^{-1}$, a phase of $\phi_3=0$, and $\tau_3=400$ fs, respectively. The coupling constants were determined by fitting the room temperature linear absorption spectrum of LH2 given in Ref. 18. Since in this paper we consider the B850 band and neglect its weak coupling to the B800 band, it is simply characterized by its $\approx 470\ \text{cm}^{-1}$ width. Assuming a Gaussian inhomogeneous distribution of molecular frequencies Ω_n [cp. Eq. (5)] with a FWHM of $\sigma=527\ \text{cm}^{-1}$,[34] we find that for models I, II, and III a coupling constant $\lambda=381\ \text{cm}^{-1}$ leads to a good agreement of the linear absorption linewidth with experiment[18], see Fig. 2(a). The oscillations of $M(t)$ and $g(t)$ [see Fig. 2(b)] in model III result in weak modulations of the absorption spectrum. The value $\lambda=381\ \text{cm}^{-1}$ used for all cases is smaller than the sum of the coupling constants used in Ref. 18. This has two reasons: (1) unlike in Ref. 18 we have incorporated disorder in our

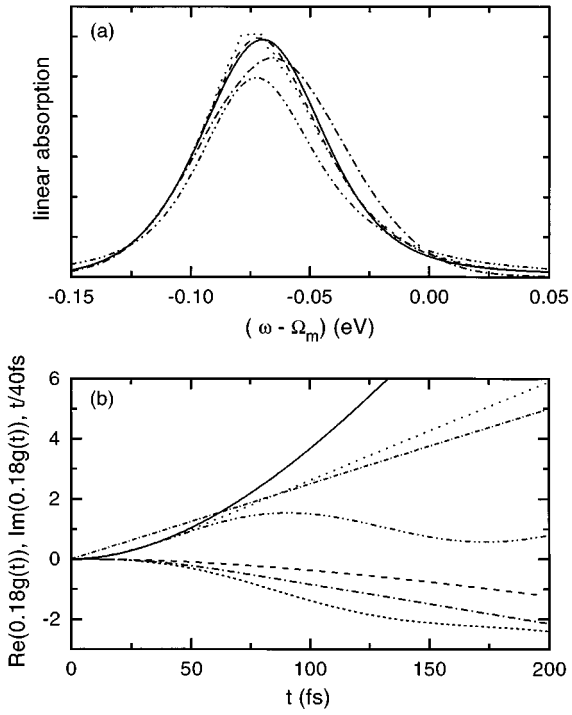

FIG. 2. (a) Linear absorption for models I−V. Solid line: model I, dashed: II, dotted: III, dash-dot: IV, and dashed-dot-dot: V. (b) Re and Im parts of $0.18g(t)$ and $t/40$ fs as function of t. Solid line: Re$[0.18g(t)]$ for model I, dashed line: Im$[0.18g(t)]$ for model I; dotted and dash-dot: Re/Im for models II and V; dash-dot-dot and short-dash: Re/Im for model III; dash-dot: $t/40$ fs corresponding to model IV. 0.18 is the average one-exciton inverse participation ratio.

calculations, hence part of the linear absorption width is induced by disorder (inhomogeneous dephasing), which therefore reduces the homogeneous contribution. (2) The incorporation of excitonic effects leads to the participation ratio factors in front of $g(t)$, see Eqs. (50) and (51), which are smaller than one, and therefore would require an increase of the coupling strength to maintain the same linewidth. The smaller coupling strength compared to Ref. 18 shows that for determining the linear absorption the disorder [which also increases the excitonic participation ratio due to localization and therefore reduces effect (2)] is more important than the exciton-phonon coupling. This justifies the application of our theory, based on the neglect of the Hamiltonian H_1, to the highly disordered B850 band of LH2.

To pinpoint the effects of the disorder-induced correlation length we consider model IV, which has the same spectral density of model II, but with the independent molecular disorder replaced by a correlated Gaussian inhomogeneous broadening of the molecular transition frequencies Ω_n [Eq. (5)], which results in a correlated Gaussian inhomogeneous broadening of the exciton energies ϵ_μ [Eq. (13)] with the same FWHM $\sigma=527$ cm^{-1}. Replacing the disorder with short correlation length (models I−III) with the simple inhomogeneous broadening of model IV does not significantly influence the linear absorption linewidth [see Fig. 2(a)], but shifts its maximum towards the blue, since in model IV, unlike in models I−III, no disorder-induced localization takes place.

To further demonstrate the importance of the proper inclusion of exciton-phonon coupling via the spectral densities, we introduce model V, where we include independent molecular disorder as in models I−III, but replace $g(t)$ by a simple homogeneous dephasing Γt, which corresponds to the limit $M_V(t)\propto\delta(t)$, neglecting the imaginary parts of $g(t)$, and assuming the same dephasing for all transitions, i.e. setting all the participation ratio factors in front of $g(t)$ to 1. The calculated linear absorption spectrum is very close to models I and II, see Fig. 2(a). The fact that the maximum of the absorption for model V appears at about the same position as for model I, II, and III, proves again that the ≈ 560 cm^{-1} redshift of the aggregates absorption compared to the monomer absorption (Ω_m) shown in Fig. 2(a), results primarily from excitonic and disorder effects and not from the exciton-phonon coupling.

The calculation of the linear absorption, presented in Fig. 2(a), required the averaging over 10,000 realization of disorder to produce convergent results. In the calculation of the following FWM signals we have used 1000 realizations, which for the rather short times and time-delays considered here, are sufficient. If one is interested in the dynamics for longer times or time-delays this number needs to be increased considerably, to properly take into account all interferences that may be present in the signals.

In the absence of disorder or for correlated disorder (model IV) due to the geometry of LH2 with a tangential head to tail orientation of the dipoles, the lowest exciton carries no oscillator strength.[45] The next higher two excitons (characterized by wavevectors $k=\pm\pi/N$) are degenerate and bright and carry almost the entire oscillator strength of the aggregate. With disorder the picture changes and for each realization of disorder about five excitons carry significant oscillator strength.[34,37]

To connect our results with experiment[18] we now discuss the time-integrated FWM signals, see Eq. (43). Figures 3(a)–3(e) display the time-integrated FWM signals for our five models. For each model the total signal and the four contributions A, B, C, and D are shown. The time-integrated signals for models I, II, and III [Figs. 3(a)–3(c)] are very similar. For negative τ only the two-exciton contributions C and D are present. Due to their different signs they strongly cancel resulting in a total signal much weaker than the two contributions. Due to the presence of disorder, in all cases I, II, and III the signal decreases rapidly with increasing negative τ. At $\tau=0$ the signal shows a discontinuity, reflecting the sudden appearance of the one-exciton contributions A and B, which are only finite for $\tau>0$, and the disappearance of D, which exists only for negative τ. Similar step-like signatures in the time-integrated FWM signals around $\tau=0$ have been predicted and observed in semiconductor quantum wells,[61] where the relevant two-exciton states are bound two-exciton states, i.e., biexcitons. In Ref. 61, however, the signals for negative time delays were more pronounced, since the quantum well investigated in the experiment had only a small inhomogeneous broadening. So far, no two- or three

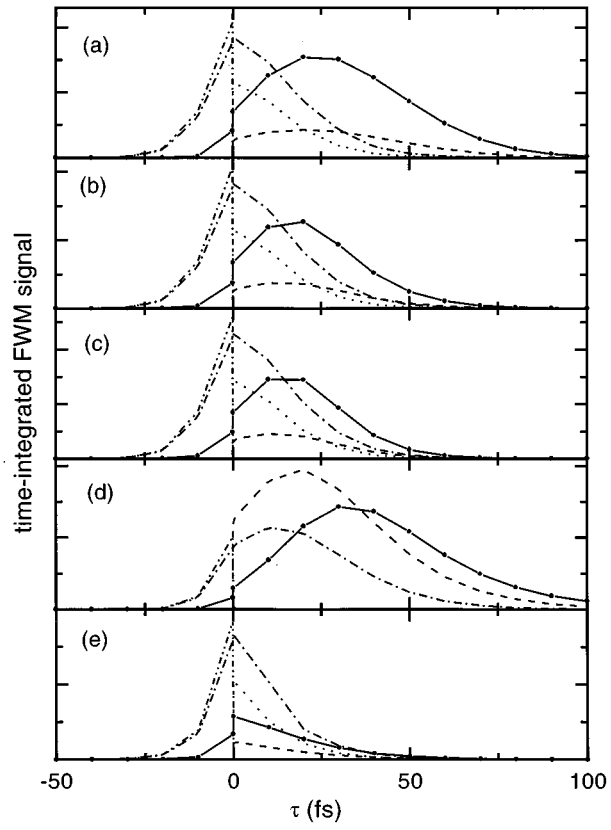

FIG. 3. Time-integrated four-wave-mixing signal $S_{\mathrm{INT}}(\tau)$ [Eq. (43)]. (a) For model I, (b) model II, (c) model III, (d) model IV, and (e) model V. Solid lines: total polarization, dashed lines: A ($A+B$ for model IV), dotted lines: B, dash-dot C, and dash-dot-dot: D. The circles indicate the values of τ which have been used to calculate the polarization, the lines are guides for the eyes. For better visibility the values for the total polarization have been multiplied by 5.

pulse echo experiments have been reported for the B850 band of LH2. However, the FWM signals for LH1[18] and for the B800 band of LH2[17] show only weak signals for negative time delays, reflecting the strong disorder in these samples. For a quantitative comparison with experiment, the finite laser pulse duration should be included in the theory, since it is clear that finite pulses will smooth the features shown in Fig. 3 around $\tau=0$ and will also reduce the contribution of two-exciton states relative to the one-exciton contributions, since the two-exciton band is very broad. In addition, the third molecular level, which is close in energy to the lowest two-exciton states and has not been included in the present study should be considered. Due to the coupling of this third level to the two-exciton states, one can expect Fano-resonances, which have distinct signatures in four-wave-mixing signals,[62] and which may, depending on the details of the couplings and the excitation conditions, reduce or enhance the contributions of two-exciton states.

With increasing positive τ the total signal rises, reaches a maximum at $\tau\approx 20$ fs and subsequently decays. Precise comparison with experiment is not straightforward and requires the inclusion of finite pulse effects. The position of the maximum is close to the maximum observed in Ref. 18 for zero intermediate time delay, i.e. when the three-pulse experiment coincides with the two-pulse experiment, which was ≈ 25 fs using 35 fs laser pulses. Comparing the temporal profiles of A, B, and C we see that B and C are larger than A for small τ, but decay much more rapidly with increasing τ. This difference is caused by disorder, which induces a strong dephasing of the contributions B and C and the buildup of the photon-echo of A has been discussed in the previous section and this will be illustrated later for the time-resolved signals. Due to this buildup, A reaches a maximum at a certain τ which is approximately given by the half the temporal width of the time-resolved signal. At large $\tau>50$ fs for model I and II, B and C are small and the total signal is close to A. For model III the modulation of $g(t)$ [cp. Fig. 2(b)] results in a very weak modulation of the time-integrated FWM signal.

To isolate the effects of disorder, we compare the time-integrated signals which are similar for models I, II, and III, with model IV, where we replaced the independent distribution functions for the molecular frequencies by a correlated-disorder [see Eq. (64)], assuming the same frequency fluctuation on each molecule. For this model, since for the LH2 geometry there are basically only two degenerate excitons with a significant oscillator strength, the distinction between A and B depends on the basis set and is therefore arbitrary. In the figures associated with model IV we therefore combine these contributions. It is important to stress that the theory developed in this paper describes disordered aggregates in which due to exciton localization, interacting (overlapping) excitons are separated energetically. This implies that the theory based upon the neglect of H_1 [see Eq. (12)], may not be applicable to the highly ordered model with degenerate excitons delocalized over the entire aggregate. For negative τ the time-integrated signal for model IV shown in Fig. 3(d) decays about as rapidly as for the previous models. For positive delays there are, however, distinct differences; due to the ideal correlation of the disorder in this case all contributions are emitted as photon-echoes and reach a maximum at some finite τ.

Figure 3(e) shows the time-integrated signal for model V. For negative delays, due to disorder, the signal again decays very rapidly. For positive delays the signals do not show a maximum at finite τ but decay very rapidly. Even though the linear absorption linewidth is essentially the same, as in the models which included $g(t)$, the FWM signal in the homogeneous limit decays very rapidly. This difference is related to the different temporal behavior induced by $g(t)$. In Fig. 2(b) the line shape functions, which have been multiplied by 0.18 [this is the average one-exciton inverse participation ratio, which enters as a prefactor, see Eq. (50)] and $t/40$ fs are displayed. Instead of being linear in time, $\mathrm{Re}[g(t)]$ and $\mathrm{Im}[g(t)]$ used in models I, II, and III are quadratic for the times of interest, which implies that for the parameters used here, the limit of slow nuclear dynamics applies. We also see that $|\mathrm{Im}[g(t)]|<|\mathrm{Re}[g(t)]|$ which so the Stokes shift is small compared to the dephasing caused by $g(t)$. This is in agreement with the linear absorption [Fig.

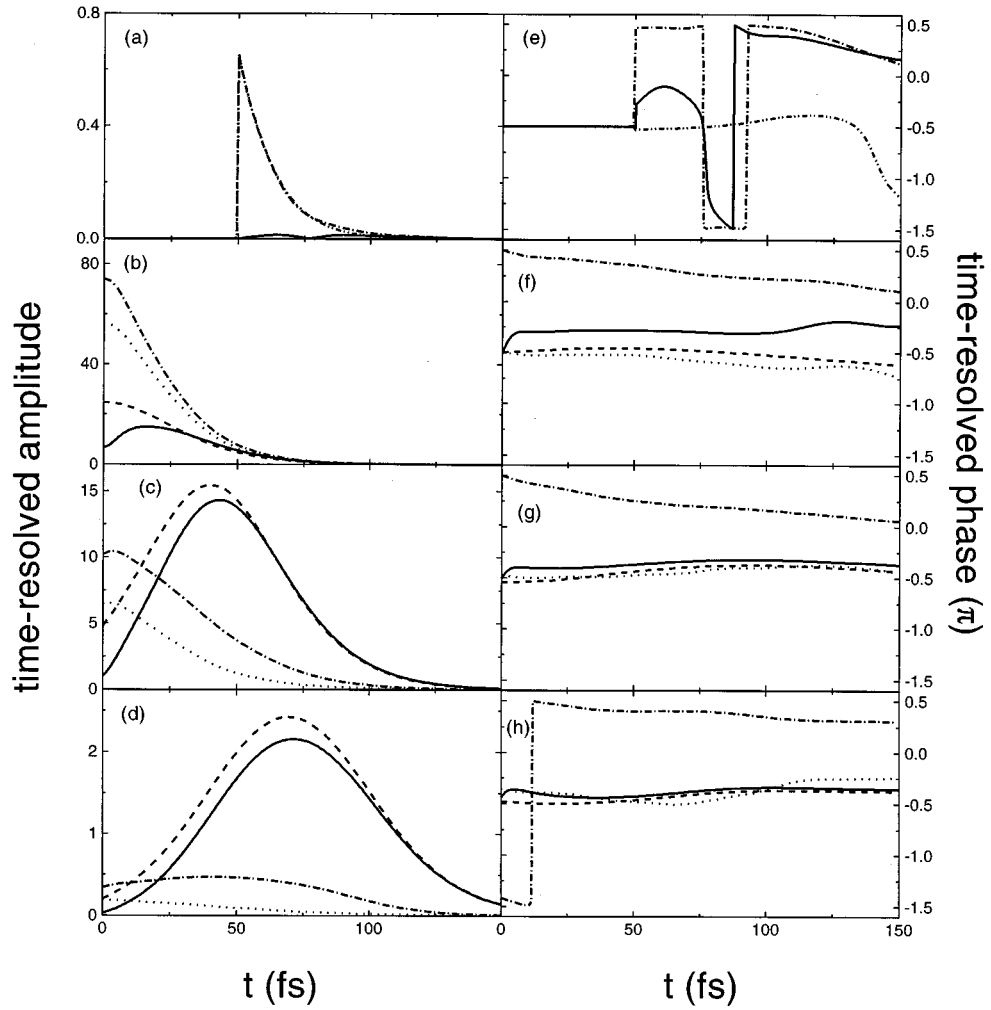

FIG. 4. Time-resolved amplitude (a)–(d) and phase (e)–(h) of four-wave-mixing polarization $S_0(t,\tau)$ [Eq. (35)] for model I for $\tau=-50$ (a) and (e), 0 fs (b) and (f), 50 fs (c) and (g), and 100 fs (d) and (h) with $\tilde{\omega}=\Omega_m-560$ cm^{-1}. Solid lines: total polarization, dashed lines: *A*, dotted lines: *B*, dash-dot *C*, and dash-dot-dot: *D*.

2(a)], where it is shown that the maximum occurs at almost the same position for models I, II, and III [which included $g(t)$], and model V, where a homogeneous dephasing $\exp[-t/40$ fs] has been assumed, neglecting the imaginary part of $g(t)$.

We now discuss time-resolved FWM, the spectrally resolved FWM, and the WS for the various models. The time-resolved amplitude and phase $\varphi(t,\tau)$ [see Eq. (35)] of the FWM signal for model I are displayed in Figs. 4(a)–4(h). Figures 5, 6, 7, and 8 contain the same quantities for models II, III, IV, and V, respectively. A different perspective on these quantities is provided by the contour plots of the dynamics of amplitude versus t and τ for our models I, III, IV, and V given in the left column of Fig. 9 (from top to bottom). The right column gives the corresponding phases of the signal (Model II is not given since it is very similar to model I). Instead of analyzing the temporal (amplitude) and spectral (phase) dynamics separately, it is possible to introduce the WS, which simultaneously displays both type of information. The WS for models I, III, IV, and V are displayed in Fig. 10 (from top to bottom) for four different delays, as indicated.

Using Figs. 4–10 we next compare the behavior of all models. For model I at $t=\tau=0$, see Fig. 4(d), the contributions A and B have a phase of $-\pi/2$, which means that the excitation like in a simple two-level system follows the exciting pulses with this phase shift.[54,59] Due to the $-$ sign [cp. Eqs. (46) and (47)] which represents a phase shift of π, C has initially a phase of $\pi/2$. [see Figs. 4(f), 5(f), 6(f), 7(f), and 8(f)]. For $\tau=-50$ fs the signal is solely determined by terms involving two-exciton states C and D. Since these terms differ only in the last interaction (cp. diagrams displayed in Fig. 1) they are very similar, and cancel strongly due to their different sign, resulting in a small overall signal [Fig. 4(a)]. To display the phase dynamics we have chosen $\tilde{\omega}=\Omega_m-0.07$ eV [see Eqs. (35)], where Ω_m is the average molecular transition frequency, which is close to the linear absorption maximum, see Fig. 2(a). Since the strongest transitions between the one- and two-exciton states do not spec-

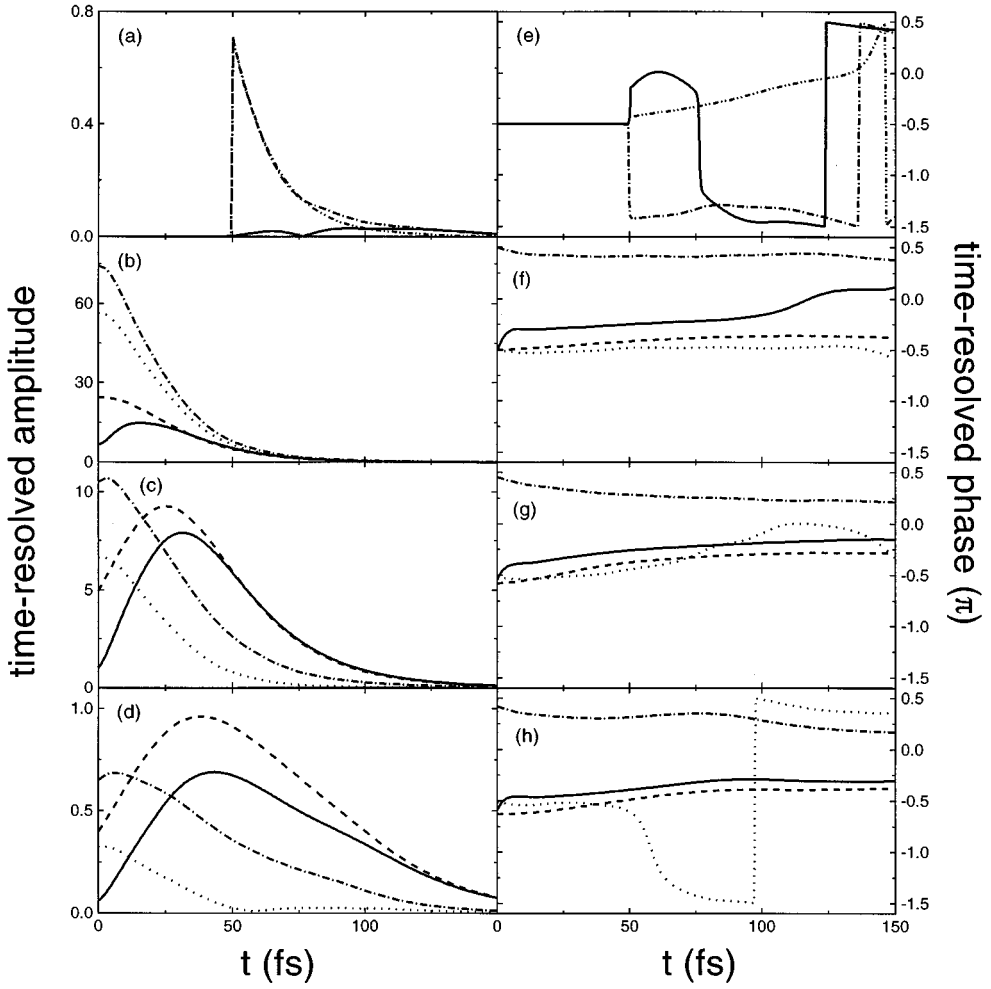

FIG. 5. Time-resolved amplitude (a)–(d) and phase (e)–(h) of four-wave-mixing polarization $S_0(t,\tau)$, for model II for $\tau=-50$ (a) and (e), 0 fs (b) and (f), 50 fs (c) and (g), and 100 fs (d) and (h) with $\tilde{\omega}=\Omega_m-560$ cm^{-1}. Solid lines: total polarization, dashed lines: *A*, dotted lines: *B*, and dash-dot *C*, and dash-dot-dot: *D*.

trally match with the absorption maximum and due to the cancellation between terms C and D, we observe a rapid phase dynamics, see Fig. 4(e). For $\tau=0$ fs A, B, and C contribute to the signal. Figures 4(b) and 4(f) display the dynamics of the amplitude and phase of the three contributions as well as the total signal. While the amplitudes of all three terms A, B, and C decay with time, due to the cancellation between the terms for short times the total amplitude of the signal is small. It then increases and at about $t=20$ fs reaches a maximum, whose position is determined by the homogeneous dephasing and also by the dephasing between the one- and two-exciton contributions caused by their different frequencies. For longer times it subsequently decays. The different signs of contributions A and B compared to C result in a corresponding change of phase. While for A and B the phase starts with $-\pi/2$ at $t=0$, C has a phase of $\pi/2$, see Fig. 4(f). For longer time delays $\tau=50$ fs and $\tau=100$ fs the buildup of an echo-like structure can be seen for A and the total signal, see Figs. 4(c) and 4(d). However, due to the presence of homogeneous dephasing, the position of the maximum of the time-resolved amplitude is not exactly given by the time delay τ, but shows up at shorter times, for $\tau=100$ fs for example at about $t\approx 70$ fs.

To obtain a more complete picture of the time-resolved response, the first row of Fig. 9 displays contour-plots of the dynamics of the amplitude (left column) and the phase (right column) versus t and τ. Figure 9 clearly shows the signals occurring for negative τ and the shift of the maximum of the time-resolved signal to longer times (shorter than τ) with increasing time delay. Further Fig. 9 displays the rapid (slow) dynamics of the phase occurring for negative (positive) τ.

The first row of Fig. 10 shows the WS for $\tau=-50,\ 0,\ 50,\ 100$ fs. For positive delays the signals are quite symmetric with respect to the detuning around $\omega=\Omega_m-560$ cm^{-1} and have a positive (blue) maximum following the last pulse at this spectral position. This is a direct consequence of the slow dynamics of the phase (Fig. 4). The maximum of the WS appears at longer times with increasing τ as shown by the time-resolved signals. For negative time

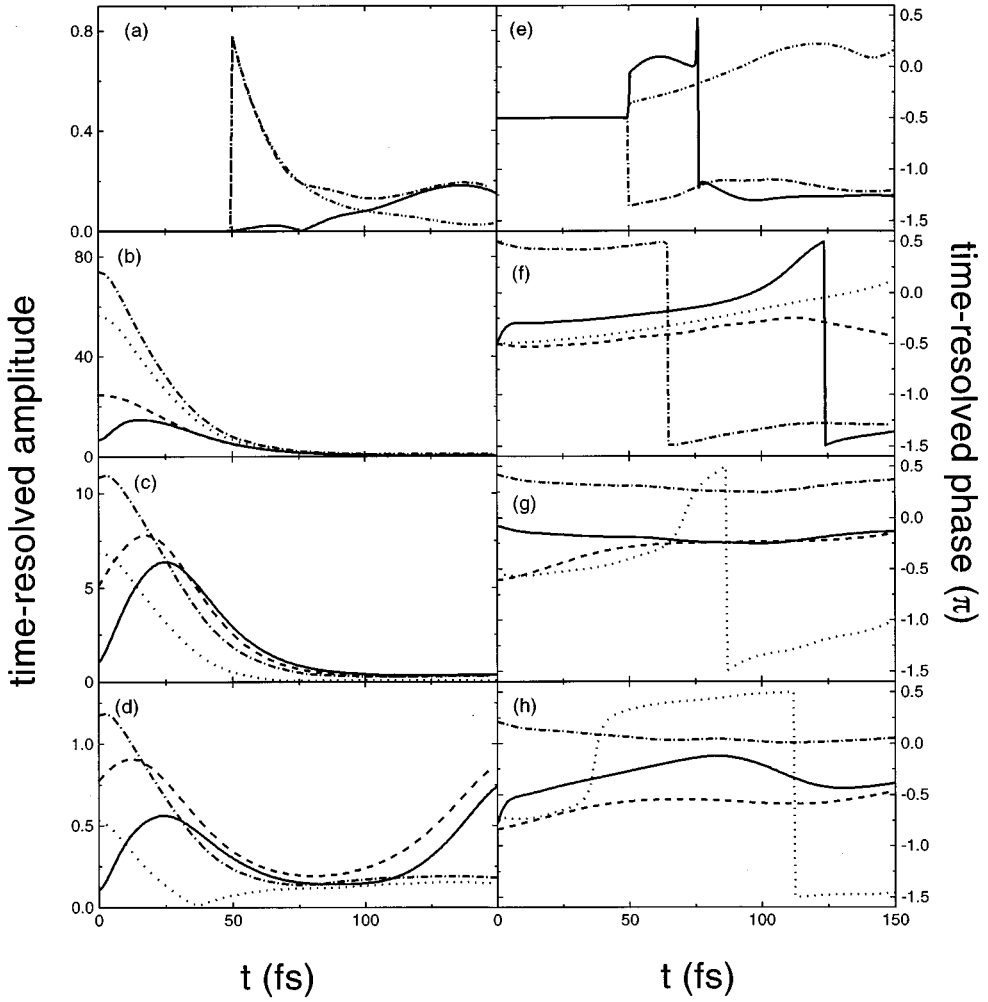

FIG. 6. Time-resolved amplitude (a)–(d) and phase (e)–(h) of four-wave-mixing polarization $S_0(t,\tau)$, for model III for $\tau=-50$ (a) and (e), 0 fs (b) and (f), 50 fs (c) and (g), and 100 fs (d) and (h) with $\tilde{\omega}=\Omega_m-560\ \mathrm{cm}^{-1}$. Solid lines: total polarization, dashed lines: A, dotted lines: B, dash-dot C, and dash-dot-dot: D.

delay, due to the rapid dynamics (chirp) of the phase the initial value of the WS around $\omega=\Omega_m-560\ \mathrm{cm}^{-1}$ following the last pulse is negative. For longer times the maximum of the WS shifts slightly towards the red.

The only difference between models I and II is that we replaced the exponential $M(t)$ by a Gaussian. As shown in Fig. 2(b) the resulting $g(t)$ are very similar for times shorter than ≈ 50 fs and we therefore also expect similar FWM signals for these two models. This is confirmed by the very similar time-integrated signals shown in Figs. 3(a) and 3(b), and also by comparing the time-resolved signals displayed in Fig. 5 with the ones for model I Fig. 4.

Comparing models I and II with model III the picture changes somewhat, since the oscillating 190 cm^{-1} nuclear mode included in III, results in oscillations of $g(t)$ with a time period of about $t_B\approx 175$ fs [see Fig. 2(b)], also the FWM signals are weakly modulated. For $\tau=0$ and 50 fs these modulations are not very pronounced since the time-resolved signal reaches its maximum close to the last pulse and since the time period of the oscillation is longer than the decay time of the FWM signal. For $\tau=100$ fs we, however, see a strong influence of the modulation. Due to the modulation of $g(t)$, the time-resolved signal [Fig. 6(b)] does not have its maximum around $t\approx 70$ fs as for model I, but rather has a minimum at this time and shows maxima for shorter and longer times. This amplitude- and phase-modulation induced by the oscillating nuclear mode can be clearly seen in the contour-plots in the second row of Fig. 9 and in the WS displayed in the second row of Fig. 10. The maximum of the WS for $\tau=-50$ fs the maximum appears at rather long times, in agreement with the time-resolved signal [see Fig. 6(a)]. For $\tau=100$ fs (see Fig. 10) around $t=80$ fs, which corresponds to the maximum of the time-resolved signal [see Fig. 6(d)], strong modulations of the WS as function of detuning with a period close to the frequency of the oscillating nuclear mode appear. Apart from these modulations and a somewhat slower decay, the time-integrated FWM signal [Fig. 3(c)] and the time-resolved signals for model III (Fig. 6) look for positive $\tau<50$ fs qualitatively similar to those obtained for models I and II.

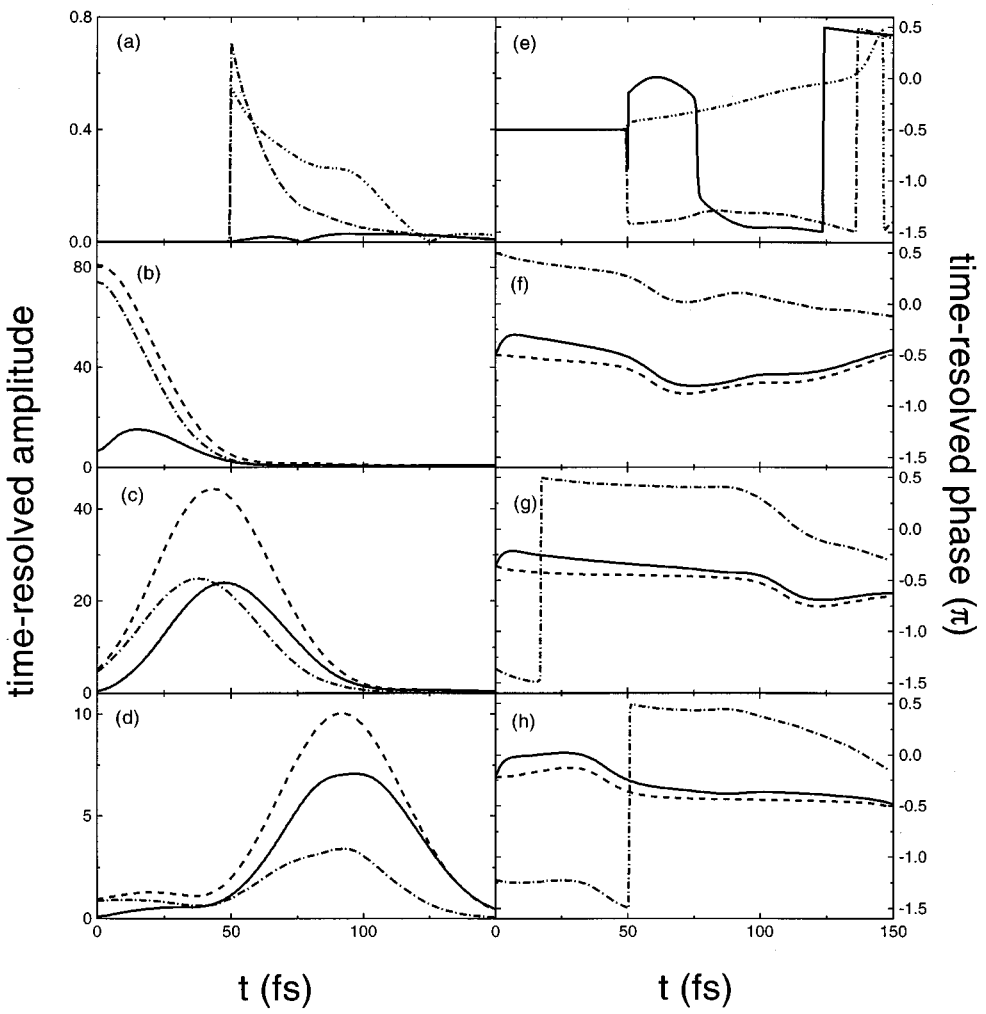

FIG. 7. Time-resolved amplitude (a)–(d) and phase (e)–(h) of four-wave-mixing polarization $S_0(t,\tau)$, for model IV for $\tau=-50$ (a) and (e), 0 fs (b) and (f), 50 fs (c) and (g), and 100 fs (d) and (h) with $\tilde{\omega}=\Omega_m-560$ cm^{-1}. Solid lines: total polarization, dashed lines: $A+B$, dash-dot C, and dash-dot-dot: D.

While for models I, II and III, which all included homogeneous dephasing via $g(t)$ and a disorder with a short correlation length, the FWM signals are very similar, the situation is different for model IV where we used the same $g(t)$ as in model II, but assumed a disorder with a long correlation length. Due to the correlated disorder in this model, as shown in Fig. 7 all contributions present for positive τ A $+$B, C, and the total signal are emitted as photon echoes. For longer τ the maximum of the time-resolved amplitude occurs close to τ [see Fig. 7(d)], which can also be seen in the contour-plot in the left column of the third row of Fig. 9. The right column shows that as in disordered two-level systems for positive τ, the phase of the time-resolved signal follows $t\propto\tau$ lines. The rapid phase dynamics shown in Figs. 7(e)–7(h) comes basically from the shift of the energy levels compared to model I$-$III, due to the absence of exciton localization which is induced by short range disorder [cp. Fig. 2(a)].

We also find dramatic differences between models I$-$III and model V, where $g(t)$ has been replaced by $t/40$ fs, i.e., by a simple exponential decay. Due to the homogeneous limit the dephasing changes from a Gaussian form at short times to an exponential [see Fig. 2(b)], which decays more rapidly at short times. Therefore for the homogeneous limit assumed in model V the time-integrated (see Fig. 3) and also the time-resolved signals A, B, and C (see Fig. 8), decay very rapidly. In the time-resolved signals (A) only a very broad echo-like feature can be observed for $\tau=100$ fs. Due to the cancellation between the one- and the two-exciton contributions, the total time-resolved signals have their maxima with some delay after the last pulse, see Figs. 8(b)–8(d). We have demonstrated very different FWM signals for models with very similar linear absorption. Due to the rather rapid decay, the spectrograms shown in the fourth row of Fig. 10 reach their maxima slightly earlier compared to model I.

VII. SUMMARY

In this paper we have investigated femtosecond two-pulse four-wave-mixing signals from molecular aggregates.

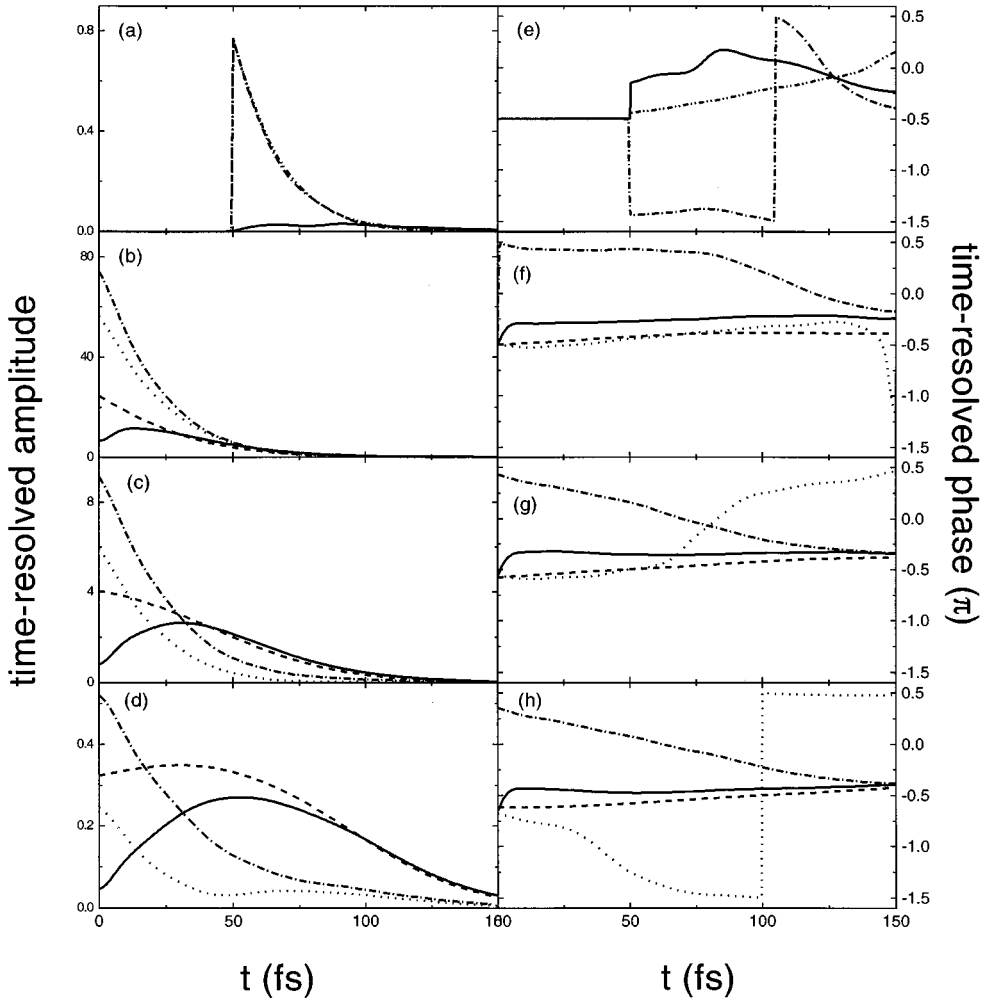

FIG. 8. Time-resolved amplitude (a)–(d) and phase (e)–(h) of four-wave-mixing polarization $S_0(t,\tau)$, for model V for $\tau=-50$ (a) and (e), 0 fs (b) and (f), 50 fs (c) and (g), and 100 fs (d) and (h) with $\tilde{\omega}=\Omega_m-560\ \mathrm{cm}^{-1}$. Solid lines: total polarization, dashed lines: *A*, dotted: *B*, dash-dot *C*, and dash-dot-dot: *D*.

The present model includes exciton-phonon interactions represented by arbitrary spectral densities, static disorder, and two-exciton states. All of these effects have distinct signatures in four-wave mixing which have been discussed in Sec. V using simple excitonic two-, three-, and four-level systems. In Sec. VI we have applied the theory to the B850 band of LH2. Results for various time-integrated and time-resolved four-wave-mixing and Wigner spectrogram have been presented, and have been connected to experiments using time-integrated detection.[18] We predict the lineshapes and phase dynamics of time-resolved experiments. As discussed in Sec. VI the outcome of such experiments could be used to determine the strength and the type of disorder present in the system. These measurements should also be very sensitive to exciton-phonon dynamics, which enter as dephasing and also as modulations of the transition frequencies.

Photon echoes are traditionally analyzed using a two-level model and the corresponding fast (homogeneous) versus slow (inhomogeneous) contributions to the linewidth. This model is not applicable for aggregates where the signals depend on the combined effects of excitonic structure, exciton-phonon coupling, and static disorder. In addition, solvent and protein nuclear vibrations are characterized by broad spectral densities with a multitude of timescales which are not necessarily ''slow'' or ''fast.'' The present theory allows a realistic modeling of photon echo measurements which takes all of these effects into account.

ACKNOWLEDGMENTS

The support of the Air Force Office of Scientific Research, the National Science Foundation Center for Photoinduced Charge Transfer, and the National Science Foundation through Grants No. CHE-9526125 and No. PHY94-15583 is gratefully acknowledged.

APPENDIX A: EXCITON REPRESENTATION OF SPECTRAL DENSITIES

In this Appendix we derive expressions for collective bath coordinates and dipole matrix-elements in the exciton

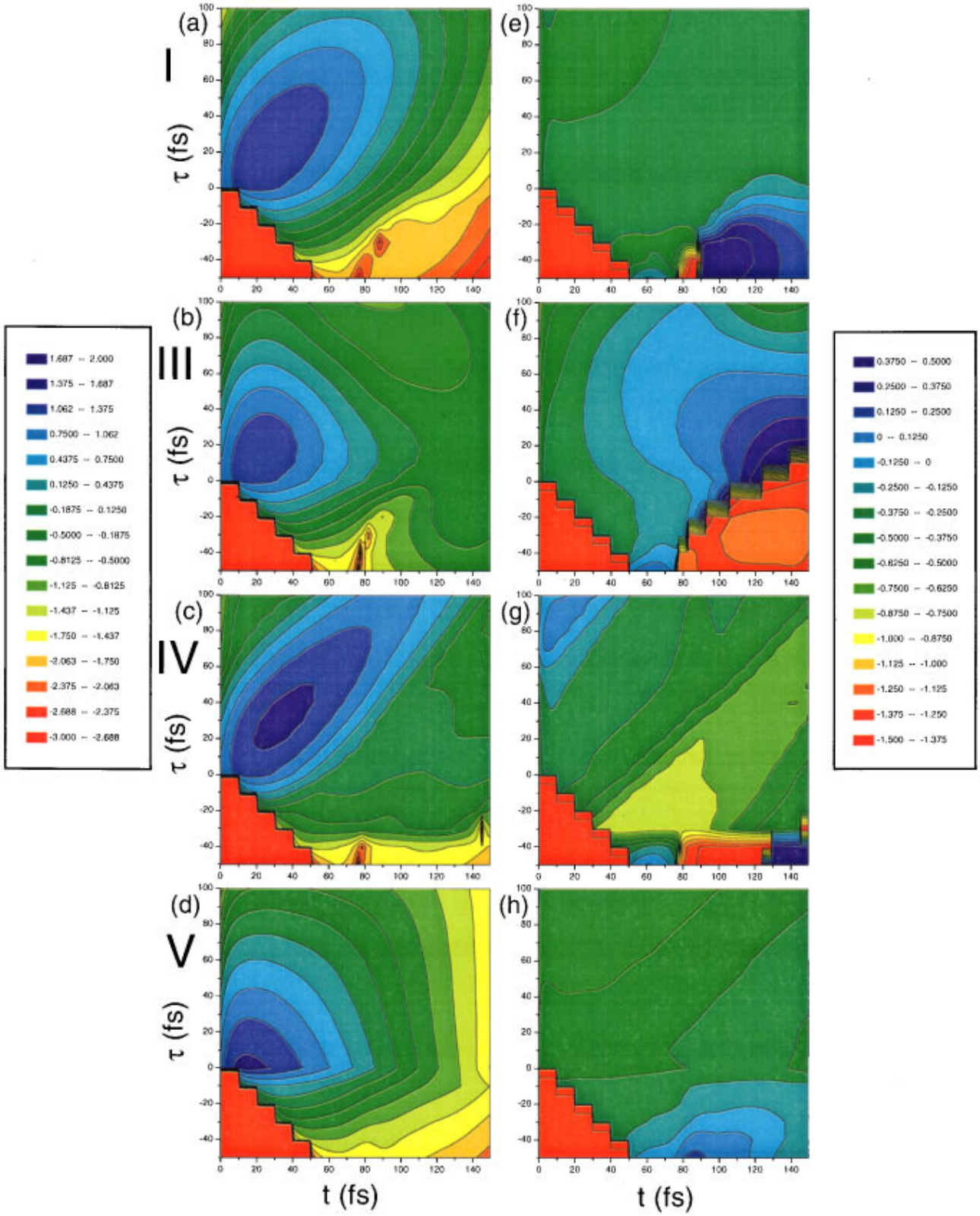

FIG. 9. Left column: (a)–(d) logarithm of amplitude of four-wave-mixing polarization $S_0(t,\tau)$ for models I, III, IV, and V (from top to bottom). Right column: (e)–(h) phase of $S_0(t,\tau)$ in units of π for the same models.

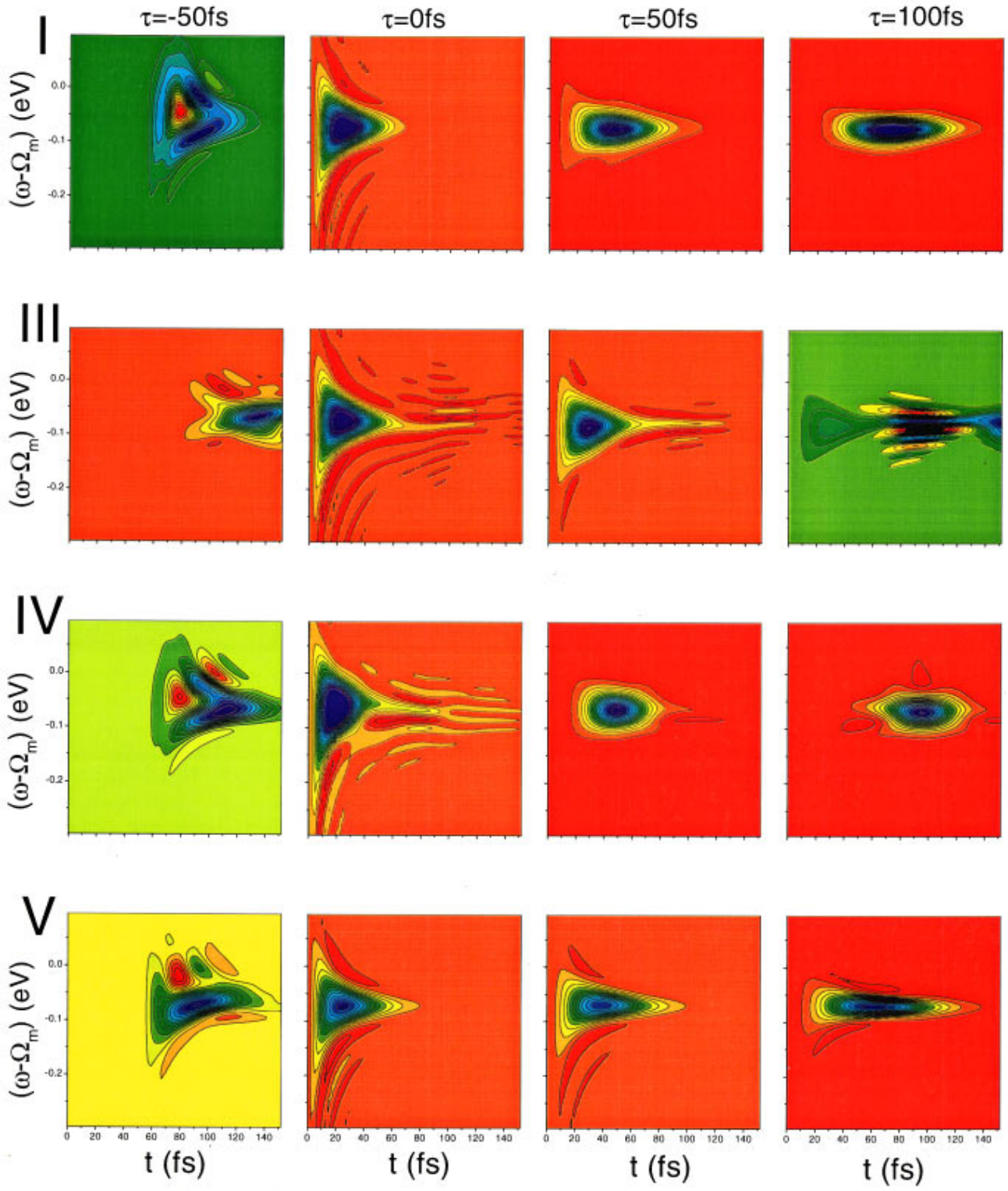

FIG. 10. Wigner spectrograms for models I, III, IV, and V (from top to bottom) for four different time delays $\tau = -50$, 0, 50, and 100 fs (from left to right). The color codes (which are different for each panel) are similar to Fig. 9, large(positive)=blue, green, yellow, red=small(negative).

representation which enter Eqs. (12)–(13). We also express the spectral densities in the exciton representation in terms of molecular spectral densities.

Expressions for collective coordinates can be obtained by projecting the second term in the r.h.s. of Eq. (4) into the subspace of one- and two-exciton states, which yields

$$
\begin{aligned}
q_{\mu}^{(c)} &= \sum_{mn} \varphi_{\mu}(m)\varphi_{\mu}(n)q_{mn}^{(c)}, \\
q_{\mu\nu}^{(c)} &= \sum_{mn} \varphi_{\mu}(m)\varphi_{\nu}(n)q_{mn}^{(c)}, \\
q_{\bar{\mu}}^{(c)} &= \sum_{mns} q_{mn}^{(c)}[\Psi_{\bar{\mu}}(m,s)+\Psi_{\bar{\mu}}(s,m)]^2, \\
q_{\bar{\mu}\bar{\nu}}^{(c)} &= \sum_{mns} q_{mn}^{(c)}[\Psi_{\bar{\mu}}(m,s)+\Psi_{\bar{\mu}}(s,m)] \\
&\quad \times[\Psi_{\bar{\nu}}(n,s)+\Psi_{\bar{\nu}}(s,s)].
\end{aligned}
\tag{A1}
$$

The one-exciton wavefunctions $\varphi_{\mu}(m)$ and the two-exciton wavefunctions $\Psi_{\overline{mu}}(m,n)$ are chosen to be real with $\Psi_{\overline{mu}}(m,m)=0$, and are normalized as

$$
\begin{aligned}
&\sum_{m} |\varphi_{\mu}(m)|^2 = 1, \\
&\sum_{mn} \Psi_{\bar{\mu}}(m,n)[\Psi_{\bar{\mu}}(m,n)+\Psi_{\bar{\mu}}(n,m)] = 1.
\end{aligned}
\tag{A2}
$$

Note that the two-exciton wavefunctions $\Psi_{\bar{\mu}}(m,n)$ can be chosen to be symmetric with respect to exchange of m and n, but this is not assumed here. The dipoles d_{μ}, $d_{\mu,\bar{\mu}}$ can be obtained by evaluating matrix elements of the polarization operator between the ground state and one-exciton and two-exciton states, resulting in

$$
\begin{aligned}
d_{\mu} &= \sum_{m} d_m \varphi_{\mu}(m), \\
d_{\mu,\bar{\mu}} &= \sum_{mn} \Psi_{\bar{\mu}}[\varphi_{\mu}(m)d_n+\varphi_{\mu}(n)d_m].
\end{aligned}
\tag{A3}
$$

Expressions for the spectral densities follow immediately from Eqs. (A1). Using a natural notation $C_{\mu\nu}\equiv C_{\mu\mu,\nu\nu}$, $C_{\bar{\mu}\bar{\nu}}\equiv C_{\overline{\mu\mu},\overline{\nu\nu}}$, $C_{\mu\bar{\nu}}\equiv C_{\mu\mu,\overline{\nu\nu}}$, $C_{\mu,\alpha\beta}\equiv C_{\mu\mu,\alpha\beta}$, $C_{\mu,\bar{\alpha}\bar{\beta}}\equiv C_{\mu\mu,\overline{\alpha\beta}}$, $C_{\bar{\mu},\alpha\beta}\equiv C_{\overline{\mu\mu},\alpha\beta}$, $C_{\bar{\mu},\bar{\alpha}\bar{\beta}}\equiv C_{\overline{\mu\mu},\overline{\alpha\beta}}$ and introducing the linear transformation which connects matrix elements of $q^{(c)}$ in molecular and exciton representation with matrix elements

$$
\begin{aligned}
A_{\mu\nu,mn} &\equiv \varphi_{\mu}(m)\varphi_{\nu}(n), \\
\overline{A_{\bar{\mu}\bar{\nu},mn}} &\equiv \sum_{s} [\Psi_{\bar{\mu}}(m,s)+\Psi_{\bar{\mu}}(s,m)][\Psi_{\bar{\nu}}(n,s) \\
&\quad +\Psi_{\bar{\nu}}(s,n)],
\end{aligned}
\tag{A4}
$$

we obtain:

$$
\begin{aligned}
C_{\mu\nu,\alpha\beta}(\omega) &= \sum_{mnm'n'} A_{\mu\nu,mn}A_{\alpha\beta,m'n'}C_{mn,m'n'}(\omega), \\
C_{\mu\nu,\bar{\alpha}\bar{\beta}}(\omega) &= \sum_{mnm'n'} A_{\mu\nu,mn}A_{\overline{\alpha\beta},m'n'}C_{mn,m'n'}(\omega), \\
C_{\bar{\mu}\bar{\nu},\bar{\alpha}\bar{\beta}}(\omega) &= \sum_{mnm'n'} A_{\overline{\mu\nu},mn}A_{\overline{\alpha\beta},m'n'}C_{mn,m'n'}(\omega).
\end{aligned}
\tag{A5}
$$

APPENDIX B: THE BETHE ANSATZ FOR MULTI-EXCITON STATES

In this Appendix we present expressions for multi-exciton states in a cyclic Frenkel-exciton model with nearest-neighbor intermolecular interactions. To obtain these states we consider instead of a cyclic aggregate containing N molecules with interaction constants $J_{m,m\pm1}$ an infinite periodic one-dimensional aggregate model by defining $\Omega_{m+nN}\equiv\Omega_m$, $J_{m+nN,m\pm1+nN}\equiv J_{m,m\pm1}$. Let $\varphi_1(m),\ldots,\varphi_s(m)$ be a set of eigenstates of the one-exciton Hamiltonian on the infinite chain. Consider a Bethe s-exciton state defined as

$$
\begin{aligned}
|\varphi_1\ldots\varphi_s\rangle &\equiv \sum_{m_1\ldots m_s} \epsilon_{m_1\ldots m_s}\varphi_1(m_1)\ldots\varphi_s(m_s) \\
&\quad \times B_{m_1}^{\dagger}\ldots B_{m_s}^{\dagger}|0\rangle.
\end{aligned}
\tag{B1}
$$

In Eq. (B1) $\epsilon_{m_1\ldots m_s}$ is defined in the following way: $\epsilon_{m_1\ldots m_s}$ is antisymmetric with respect to permutations of $m_1\ldots m_s$ and $\epsilon_{m_1\ldots m_s}=1$ for $m_1<m_2<\ldots<m_s$. A straightforward calculation shows that the s-exciton state of Eq. (B1) is an eigenstate of the exciton Hamiltonian for an infinite chain. Alternatively Eq. (B1) can be derived using the Wigner-Jordan representation of the exciton model in terms of free fermions. Using the language of Bethe-Ansatz, the form of Bethe states given by Eq. (B1) means that the scattering amplitude S_{ij} of any pair of excitons i and j in our model is $S_{ij}\equiv-1$. To obtain multi-exciton states in a cyclic aggregate we impose periodic boundary conditions to the Bethe states given by Eq. (B1), which yields the following set of equations:

$$
\varphi_j(M+N) = (-1)^{s-1}\varphi_j(m); \quad j=1,\ldots,s. \tag{B2}
$$

Equations (B2) are obtained by moving the jth particle by N sites, the factor $(-1)^{s-1}$ reflects the scattering of the jth particle on the other $(s-1)$ particles in the process of shifting the jth particle by N sites. Equations (B2) constitute the set of Bethe equations[50] which have an unusual simple form for our model due to a very simple two-particle scattering amplitude $S_{ij}\equiv-1$ for any u and j. This results in the following boundary conditions for the one-exciton wavefunctions $\varphi_1,\ldots,\varphi_s$: they should be all periodic, i.e., $\varphi(m)=\varphi(m+N)$ if s is odd and they should be all antiperiodic, i.e. $\varphi(m)=-\varphi(m+N)$ when s is even. Introducing the sets of periodic and antiperiodic one-exciton $\varphi_1,\ldots,\varphi_N$ and $\overline{\varphi_1},\ldots,\overline{\varphi_N}$, respectively, we obtain multi-exciton states in a form

$$|\mu_1,\ldots,\mu_s\rangle=\sum_{m_1\ldots m_s}\epsilon_{m_1\ldots m_s}\varphi_{\mu_1}(m_1)\ldots\varphi_{\mu_s}(m_s)\times B^{\dagger}_{m_1}\ldots B^{\dagger}_{m_s}|0\rangle \tag{B3}$$

for odd s, and

$$|\mu_1,\ldots,\mu_s\rangle=\sum_{m_1\ldots m_s}\epsilon_{m_1\ldots m_s}\overline{\varphi_{\mu_1}}(m_1)\ldots\overline{\varphi_{\mu_s}}(m_s)\times B^{\dagger}_{m_1}\ldots B^{\dagger}_{m_s}|0\rangle \tag{B4}$$

for even s.

In practice, the functions $\varphi_\mu(m)$ and $\overline{\varphi_\mu}(m)$ can be found as eigenvectors of $N\times N$ h_{mn} ad $\overline{h_{mn}}$ defined as

$$\begin{aligned} h_{m,m}&=\overline{h}_{m,m}=\Omega_m,\\ h_{m,m+1}&=\overline{h}_{m,m+1}=J_{m,m+1},\\ \overline{h}_{m+1,m}&=\overline{h}_{m+1,m}=J_{m,m+1}, \end{aligned} \tag{B5}$$

for $m=1,\ldots,N-1$ and

$$h_{N,1}=h_{1,N}=J_{N,1},\quad \overline{h}_{N,1}=\overline{h}_{1,N}=-J_{N,1}. \tag{B6}$$

APPENDIX C: FOUR-WAVE MIXING IN AN EXCITONIC SYSTEM COUPLED TO AN OVERDAMPED BROWNIAN OSCILLATOR

In this Appendix we calculate the polarization of an aggregate coupled to an overdamped Brownian oscillator with an arbitrary relaxation timescale. In the high temperature limit, inserting Eq. (55) into Eq. (45) yields

$$S_0(t,\tau)=i^3E_1^-(E_2^+)^2\sum_{n_1,n_2,n_3=0}^{\infty}\sum_{\alpha=1}^{N}\sum_{m=1}^{N+2N(N-1)}a_{\alpha m}(t,\tau)\frac{(-X^{(1)}_{\alpha m})^{n_1}}{n_1!}\frac{(-Z^{(2,3)}_{\alpha m})^{n_2}}{n_2!}\frac{(-X^{(4)}_{\alpha m})^{n_3}}{n_3!}\times\exp[-i(\epsilon^{(1)}_{\alpha m}t-\epsilon^{(2)}_{\alpha m}\tau)]\exp[-(n_2+n_3)\Lambda t-(n_1+n_2)\Lambda|\tau|], \tag{C1}$$

with

$$\epsilon^{(1)}_{\alpha m}=\begin{cases}\epsilon_m-i\Lambda(Z^{(2,3)}_{\alpha m}+X^{(4)}_{\alpha m}), & m=1,\ldots,N\\ \overline{\epsilon}_{\mu(m)}+\overline{\epsilon}_{\nu(m)}-\epsilon_\alpha-i\Lambda(Z^{(2,3)}_{\alpha m}+X^{(4)}_{\alpha m}), & m=N+1,\ldots,N+N(N-1)\\ \epsilon_\alpha-i\Lambda(Z^{(2,3)}_{\alpha m}+X^{(4)}_{\alpha m}), & m=N+1+N(N-1),\ldots,N+2N(N-1)\end{cases}, \tag{C2}$$

and

$$\epsilon^{(2)}_{\alpha m}=\begin{cases}\epsilon_\alpha+i\Lambda(Z^{(2,3)}_{\alpha m}+X^{(1)}_{\alpha m}, & m=1,\ldots,N\\ \epsilon_\alpha+i\Lambda(Z^{(2,3)}_{\alpha m}+(\Theta(\tau)-\Theta(-\tau))X^{(1)}_{\alpha m}, & m=N+1,\ldots,N+N(N-1)\\ \overline{\epsilon}_{\overline{u(m)}}+\overline{\epsilon}_{\overline{\nu(m)}}-\epsilon_\alpha+i\Lambda(Z^{(2,3)}_{\alpha m}+X^{(1)}_{\alpha m}), & m=N+1+N(N-1),\ldots,N+2N(N-1)\end{cases},$$

where $\mu(m)$, $\overline{\mu(m)}$, $\nu(m)$, and $\overline{\nu(m)}$ run over all possible combinations of μ,ν and $\overline{\mu,\nu}=1,\ldots,N$ excluding the terms with $\mu=\nu$ and $\overline{\mu}=\overline{\nu}$, and

$$a_{\alpha m}(t,\tau)=\begin{cases}2\Theta(t)\Theta(\tau)|d_\alpha|^2|d_m|^2\exp[X^{(1)}_{\alpha m}+Z^{(2,3)}_{\alpha m}+X^{(4)}_{\alpha m}], & m=1,\ldots,N\\ -(\Theta(t)\Theta(\tau)+\Theta(t+\tau)\Theta(-\tau))d_\alpha d^{(2)}_{\mu(m)\nu(m)}d_{\alpha,\mu(m)\nu(m)}\\ \quad\times\exp[X^{(1)}_{\alpha m}+Z^{(2,3)}_{\alpha m}+X^{(4)}_{\alpha m}], & m=N+1,\ldots,N+N(N-1)\\ \Theta(t+\tau)\Theta(-\tau)d_\alpha d^{(2)}_{\overline{\mu(m)}\,\overline{\nu(m)}}d_{\alpha,\overline{\mu(m)}\,\overline{\nu(m)}}\exp[X^{(1)}_{\alpha m}+Z^{(2,3)}_{\alpha m}+X^{(4)}_{\alpha m}], & m=N+1+N(N-1),\ldots N+2N(N-1)\end{cases}, \tag{C4}$$

and

$$Y=\left(\frac{2\lambda k_BT}{\hbar\Lambda^2}-i\frac{\lambda}{\Lambda}\right), \tag{C5}$$

$$X^{(1)}_{\alpha m}=\begin{cases}Y^*(C_{\alpha\alpha}+C_{\alpha m}), & m=1,\ldots,N\\ \Theta(\tau)Y^*C^{(1)}_{\alpha,\mu(m)\nu(m)}+\Theta(-\tau)YC^{(1)}_{\alpha,\mu(m)\nu(m)}, & m=N+1,\ldots,N+N(N-1)\\ Y(C^{(2)}_{\mu(m)\nu(m),\mu(m)\nu(m)}-C^{(1)}_{\alpha,\mu(m)\nu(m)}), & m=N+1+N(N-1),\ldots,N+2N(N-1)\end{cases}, \tag{C6}$$

$$Z^{(2,3)}_{\alpha m}=\begin{cases}-Y^*C_{\alpha m}, & m=1,\ldots,N\\ Y^*(C_{\alpha\alpha}-C^{(1)}_{\alpha,\mu(m)\nu(m)}), & m=N+1,\ldots,N+N(N-1)\\ Y(C_{\alpha\alpha}-C^{(1)}_{\alpha,\mu(m)\nu(m)}), & m=N+1+N(N-1),\ldots,N+2N(N-1)\end{cases}, \tag{C7}$$

$$X^{(4)}_{\alpha m}=\begin{cases} YC_{mm}+Y^{*}C_{\alpha m}, & m=1,\ldots,N \\ Y(C^{(2)}_{\mu(m)\mu(m),\mu(m)\nu(m)}-C^{(1)}_{\alpha,\mu(m)\nu(m)}), & m=N+1,\ldots,N+N(N-1) \\ YC^{(1)}_{\alpha,\mu(m)\nu(m)}, & m=N+1+N(N-1),\ldots,N+2N(N-1) \end{cases} . \tag{C8}$$

The FWM signal given by Eqs. (45)–(47) can be written as a sum over contributions from various four-level systems, made of the ground, two one-exciton, and one two-exciton states, see Fig. 1. To analyze the signatures of the various physical processes on the FWM signal [Eq. (C1)], we study in Sec. V a series of simplified models, a two-, a three-, and a four-level system, respectively.

[1] S. Mukamel, *Principles of Nonlinear Optical Spectroscopy* (Oxford University Press, New York, 1995).
[2] R. van Grondelle, J.P. Dekker, T. Gillbro, and V. Sundström, Biochim. Biophys. Acta **1187**, 1 (1994).
[3] V. Sundström and R. van Grondelle, in *Anoxygenic Photosynthetic Bacteria*, edited by R.E. Blankenship, M.T. Madiga, C.E. Baner (Kluwer Academic, Dordrecht, 1995), p. 349.
[4] V.F. Kamalov, I.A. Struganova, and K. Yoshihara, Chem. Phys. Lett. **213**, 559 (1993).
[5] R. Gadonas, K.-H. Feller, and A. Pugzlys, Opt. Commun. **112**, 157 (1994).
[6] E. Gaizanskas, K.-H. Feller, and R. Gadonas, Opt. Commun. **118**, 360 (1995).
[7] K. Misawa, S. Machida, K. Horie, and T. Kobayashi, Chem. Phys. Lett. **240**, 210 (1995); T. Kobayashi, Mol. Cryst. Liq. Cryst. **283**, 17 (1996); K. Misawa and T. Kobayashi, Nonlin. Opt. **15**, 81 (1996).
[8] S.E. Bradforth, R. Jimenez, F. von Mourik, R. van Grondelle, and G.R. Fleming, J. Phys. Chem. **99**, 16179 (1995).
[9] R. Jimenez, S.R. Dikshit, S.E. Bradforth, and G.R. Fleming, J. Phys. Chem. **100**, 6825 (1996).
[10] H. van der Laan, Th. Schmidt, R.W. Visschers, K.J. Visscher, R. van Grondelle, and S. Völker, Chem. Phys. Lett. **170**, 231 (1990).
[11] N.R.S. Reddy, G.J. Small, M. Seibert, and P. Picorel, Chem. Phys. Lett. **181**, 391 (1991).
[12] N.R.S. Reddy, R.J. Cogdell, L. Zhao, and G.J. Small, Photochem. Photobiol. **57**, 35 (1993).
[13] C. De Caro, R.W. Visschers, R. van Grondelle, and S. Völker, J. Phys. Chem. **98**, 10584 (1994).
[14] T. Pullerits, M. Chachisvilis, and V. Sundström, J. Phys. Chem. **100**, 10787 (1996).
[15] T. Pullerits, M. Chachisvilis, M.R. Jones, C.N. Hunter, and V. Sundström, Chem. Phys. Lett. **224**, 355 (1994).
[16] V. Nagarajan, R.G. Alden, J.C. Williams, and W.W. Parson, Proc. Natl. Acad. Sci. USA **93**, 13774 (1996).
[17] T. Joo, Y. Jia, J.-Y. Yu, D.M. Jonas, and G.R. Fleming, J. Phys. Chem. **100**, 2399 (1996).
[18] R. Jimenez, F. van Mourik, J. Y. Yu, and G.R. Fleming, J. Phys. Chem. B **101**, 7350 (1997).
[19] F.C. Spano and S. Mukamel, Phys. Rev. Lett. **66**, 1197 (1991); J. Chem. Phys. **95**, 7526 (1991).
[20] V. Chernyak and S. Mukamel, Phys. Rev. B **48**, 2470 (1993); J. Chem. Phys. **100**, 2953 (1994).
[21] F.C. Spano and S. Mukamel, Phys. Rev. A **40**, 5783 (1989); Phys. Rev. Lett. **66**, 1197 (1991).
[22] N. Bloembergen, *Nonlinear Optics* (Benjamin, New York, 1965).
[23] J.R. Durrant, J. Knoester, and D.A. Wiersma, Chem. Phys. Lett. **222**, 450 (1994).
[24] M. van Burgel, D.A. Wiersma, and K. Duppen, J. Chem. Phys. **102**, 20 (1995).
[25] V. Chernyak, N. Wang, and S. Mukamel, Phys. Rep. **263**, 213 (1995).
[26] J.A. Leegwater and S. Mukamel, Phys. Rev. A **46**, 452 (1992).
[27] J. Knoester and S. Mukamel, Phys. Rep. **205**, 1 (1991).
[28] O. Dubovsky and S. Mukamel, J. Chem Phys. **95**, 7828 (1991).
[29] V. Chernyak and S. Mukamel (unpublished).
[30] R. Zwanzig, Lect. Theor. Phys. **3**, 106 (1961); Physica **30**, 1109 (1964).
[31] H. Mori, Prog. Theoret. Phys. **33**, 423 (1965); **34**, 399 (1965).
[32] A.A. Abrikosov, L.P. Gorkov, and I.E. Dzyaloshinski, *Methods of Quantum Field Theory in Statistical Physics* (Prentice-Hall, Englewood Cliffs, NJ, 1963).
[33] O. Kühn, V. Chernyak, and S. Mukamel, J. Chem. Phys. **105**, 8586 (1996).
[34] T. Meier, V. Chernyak, and S. Mukamel, J. Phys. Chem. B **101**, 7332 (1997).
[35] E.I. Rashba, Opt. Spektrosk. **2**, 75, 88 (1957).
[36] N.F. Mott and W.D. Twose, Adv. Phys. **10**, 107 (1961); V.L. Berezinskii, ZETF **65**, 1251 (1973).
[37] T. Meier, Y. Zhao, V. Chernyak, and S. Mukamel, J. Chem. Phys. **107**, 3876 (1997).
[38] G.D. Mahan, *Many-Particle Physics* (Plenum, New York, 1981).
[39] M.S. Pshenichnikov, W.P. de Boeij, and D.A. Wiersma, Phys. Rev. Lett. **74**, 674 (1995); W.P. de Boeij, M.S. Pshenichnikov, and D.A. Wiersma, Chem. Phys. Lett. **253**, 53 (1996).
[40] P. Vöhringer, D.C. Arnett, R.A. Westervelt, M.J. Feldstein, and N.F. Scherer, J. Chem. Phys. **102**, 4027 (1995); P. Vöhringer, D.C. Arnett, T.-S. Yang, and N.F. Scherer, Chem. Phys. Lett. **237**, 387 (1995).
[41] T. Joo, Y. Jia, and G.R. Fleming, J. Chem. Phys. **102**, 4063 (1995).
[42] V. Chernyak and S. Mukamel, J. Chem. Phys. **105**, 4565 (1996).
[43] V. Chernyak and S. Mukamel, Phys. Rev. Lett. **74**, 4895 (1995).
[44] V. Chernyak and S. Mukamel, Phys. Stat. Sol. (b) **189**, 67 (1995).
[45] G. McDermott, S.M. Prince, A.A. Freer, A.M. Hawthornthwaite-Lawless, M.Z. Papiz, R.J. Cogdell, and N.W. Isaacs, Nature (London) **374**, 517 (1995).
[46] A.S. Davydov, *Theory of Molecular Excitons* (Plenum, New York, 1971).
[47] S. Mukamel, Phys. Rev. A **28**, 3480 (1983).
[48] J.-Y. Bigot, M.-A. Mycek, S. Weiss, R.G. Ulbrich, and D.S. Chemla, Phys. Rev. Lett. **70**, 3307 (1993); D.S. Chemla, J.-Y. Bigot, M.-A. Mycek, S. Weiss, and W. Schäfer, Phys. Rev. B **50**, 8439 (1994).
[49] M. Koch, J. Feldmann, G. von Plessen, E.O. Göbel, P. Thomas, and K. Köhler, Phys. Rev. Lett. **69**, 3631 (1992).
[50] H.B. Tacker, Rev. Mod. Phys. **53**, 253 (1981); R.J. Baxter, *Exactly Solved Models in Statistical Mechanics* (Academic, London, 1982).
[51] N. Mott, *Metal-Insulator Transitions* (Taylor and Francis, London, 1974).
[52] S. Mukamel and R.F. Loring, J. Opt. Soc. B **3**, 595 (1986).
[53] M. Lindberg, R. Binder, and S.W. Koch, Phys. Rev. A **45**, 1865 (1992).
[54] T. Meier, S. Tretiak, V. Chernyak, and S. Mukamel, Phys. Rev. B **55**, 4960 (1997).
[55] L. Lepetit, G. Cheriaux, and M. Joffre, J. Opt. Soc. Am. B **12**, 2467 (1995); L. Lepetit and M. Joffre, Opt. Lett. **21**, 564 (1996); J.-P. Likforman, M. Joffre, and V. Thierry-Mieg, *ibid.* **22**, 1104 (1997).
[56] L. Cohen, Proc. IEEE **77**, 941 (1989).
[57] S. Mukamel, C. Calin-Ciurdariu, and V. Khidekel, IEEE J. Quant. Electron. **32**, 1278 (1996).
[58] L. Allen and J.H. Eberly, *Optical Resonances and Two-Level Atoms* (Wiley, New York, 1975).
[59] T. Meier and S. Mukamel, Phys. Rev. Lett. **77**, 3471 (1996).
[60] J. Erland and I. Balslev, Phys. Rev. A **48**, 5720 (1993).
[61] K. Bott, O. Heller, D. Bennhardt, S.T. Cundiff, P. Thomas, E.J. Mayer, G.O. Smith, R. Eccleston, J. Kuhl, and K. Ploog, Phys. Rev. B **48**, 17418 (1993).
[62] T. Meier, A. Schulze, P. Thomas, H. Vaupel, and K. Maschke, Phys. Rev. B **51**, 13977 (1995).